This document is the author's copy of:

Calculating ^{14}C mean residence times of inorganic carbon derived from oxidation of organic carbon in groundwater using the principles of $^{87}Sr/^{86}Sr$ and cation ratio mixing

By:

Daniel Magnone[1,2*], Laura A. Richards[2], Bart E. van Dongen[2], Charlotte Bryant[3], Jane A. Evans[4] and David A. Polya[2*]

[1]School of Geography and Centre for Water and Planetary Health, University of Lincoln, Brayford Pool, Lincoln, LN6 7TS, UK

[2]School of Earth and Environmental Sciences and Williamson Research Centre for Molecular Environmental Science, The University of Manchester, Williamson Building, Oxford Road, Manchester M13 9PL, United Kingdom

[3]NERC Radiocarbon Facility, Scottish Enterprise Technology Park, Rankine Avenue, East Kilbride, G75 OQF, UK

[4]NERC Isotope Geosciences Laboratory, British Geological Survey, Keyworth, Nottingham, NG12 5GG, UK

*Corresponding authors: dmagnone@lincoln.ac.uk & david.polya@manchester.ac.uk

which has been accepted for publication in *Geochimica et Cosmochimica Acta* (2019, 267, 322 -340, https://doi.org/10.1016/j.gca.2019.09.019) following the peer review process.

This version has not undergone a copy editting stage.

Highlights

- A new approach to calculate the age of oxidised organic carbon (OC) is developed.
- Proportions of sources of inorganic carbon (IC) are determined.
- The case study demonstrates IC from the oxidation of OC in a silicate Holocene aquifer.
- Radiocarbon adjustment shows IC from the oxidation of OC significantly younger than bulk IC.

Abstract

The model radiocarbon age of inorganic carbon (IC) in groundwater is a key parameter for understanding groundwater chemical history and physical processes such as groundwater residence times and flow rates. Current interpretations are based on the principle that bulk IC derives from multiple sources such as oxidation of organic carbon (OC), carbonate dissolution, and soil zone processes as well as from rainwater. Using this principle, multiple adjustment methods have been developed to calculate rainwater-related recharge ages. Additionally, where IC is assumed to predominantly be sourced from oxidised OC, the radiocarbon age of bulk IC must be similar to the oxidised OC. This is a key measurement given that OC oxidation controls the mobility of many important geochemical components such as Fe, As, Mn and U. In this instance, conventional approaches tacitly assume that the majority of IC comes from the oxidation of OC and that other sources have a negligible effect on the bulk age. In reality there are multiples source of IC which can all effect bulk radiocarbon ages. We present a new approach to calculate the age of IC derived from a specific source. This approach uses strontium isotopes ($^{87}Sr/^{86}Sr$) coupled with elemental ratios to trace and quantitfy the mixing of different sources of IC. We demonstrate the approach by calculating the model radiocarbon age of IC from the oxidation of OC for a case study of an aquifer in the Cambodian lowlands located adjacent to the Mekong river south of Phnom Penh. The results show that, although bulk IC is younger and more isotopically depleted than bulk organic carbon (OC), IC derived from oxidation of OC, has a similar age and isotopic signature to bulk OC. Furthermore, at our site the age of the IC formed from the oxidation of organic carbon predates modelled groundwater flow by at least a millennium indicating that in-aquifer oxidation is an important process, something previously questioned at the site. This shows that disentangling the origin of the constituent solutes of bulk IC is critical to the interpretation of the radiocarbon age and isotopic signature of bulk IC and that the approach represents a new approach for interpreting inorganic radiocarbon groundwater data.

1) Introduction

Groundwater is a hugely important resource for people across the world. It is widely used as a primary or supplementary source of drinking water, cleaning water, industrial water and for irrigation as well as providing critical ecosystem services (Gleeson et al., 2015). Yet these resources are vulnerable to degradation from over-extraction (Siebert et al., 2010) and contamination – both from anthropogenic (Ascott et al., 2017; Jasechko et al., 2017) and geogenic sources (Ravenscroft et al., 2009). A key parameter in the study of groundwater resources and dynamics is the model radiocarbon (^{14}C) mean residence time of inorganic carbon (IC) (Plummer and Glynn, 2013), which can be used as a tracer to better understand recharge sources and water-rock reactions impacting water composition (Fontes and Garnier, 1979; Fontes, 1992; Plummer and Glynn, 2013; Jasechko et al., 2017).

Radiocarbon dates are calculated by comparing the measured radiocarbon at the time of sampling to the "natural" radiocarbon in the atmosphere. It is based on the principle that radiocarbon in the sample will have undergone radioactive decay while atmospheric radiocarbon will remain constant, to a first approximation, since it is constantly produced in the upper atmosphere through interactions between cosmogenic radiation and ^{14}N (Anderson et al., 1947). Atmospheric carbon, in the form of CO_2, enters the carbon cycle through a range of routes, including precipitation and photosynthesis by plants (Broecker, 2010). Once equilibrium with atmospheric radiocarbon is broken through plant death and burial or precipitation entering groundwater recharge, radiocarbon will decay at a half-life of 5730 ± 40 years, but ^{12}C, the most abundant and stable carbon isotope, will not (Godwin, 1962). By comparing initial $^{14}C/^{12}C$ (A_{on}) with$^{14}C/^{12}C$ at a given time, t, (A_{sn}) the time since atmospheric equilibrium was broken can be estimated, which is the ^{14}C mean residence time (t) and is calculated by Equation 1.

Equation 1

$$t = \frac{5730 \pm 40 \text{ years}}{\log(2)} \log(\frac{A_{sn}}{A_{on}})$$

By convention, the specific activity (A_{sn}/A_{on}) is reported as a percentage of modern carbon activity (pmc) where pmc = (A_{sn}/A_{on})×100. Additionally, radiocarbon dating may be reported as absolute percent modern calculated by (A_{sn}/A_{abs})×100 where A_{abs} is the absolute international standard activity of oxalic acid, currently N.I.S.T. SRM 4990. Absolute modern, radiocarbon mean residence time is commonly reported as $\Delta^{14}C$ (‰) where $\Delta^{14}C$ =((A_{sn}/A_{on}) - 1)*1000. Here 0 ‰ is modern carbon as defined above and -1000 ‰ is almost radiocarbon dead (Stuiver and Polach, 1977; Plummer and Glynn, 2013). Due to the length of the half-life of ^{14}C, radiocarbon dating may be considered accurate

only for samples aged up to about 60,000 years. Beyond this, accuracy varies with laboratory detection limits (Walker, 2005).

The testing of atomic bombs in the late 1950s and earlier 1960s produced what is called the bomb-peak. The bomb-peak is an increased level of $\Delta^{14}C$ (‰) in 1965 far above the natural background level of 0 ‰ $\Delta^{14}C$. The exact value varies geographically and is stratified by latitude with 5 zones recognised. In the northernmost zone $\Delta^{14}C$ reaches 900 ‰ $\Delta^{14}C$, in the tropics, the value is 700 ‰ $\Delta^{14}C$ and in the southernmost zone it is 600 ‰ $\Delta^{14}C$. In all cases, the bomb peak has decayed back towards 50 ‰ $\Delta^{14}C$ by 2010 (Hua et al., 2013). The bomb-peak has two effects on the interpretation of groundwater radiocarbon, firstly it can be used as a marker itself to denote water pre and post 1950 sources (e.g. van Geen et al., 2003) but it may also alter the mean residence time of bulk IC, and due to the non-linear nature of radiocarbon dating these differences can be disproportionately large.

Radiocarbon IC mean residence times are often used to interpret groundwater recharge history, which is important for resource management. The simplest approach is to assume that IC comes entirely from rainwater and that groundwater can be represented with a piston flow model – analogous to water flowing through an inert tube. Here, the mean residence time of IC at a given position in the aquifer conceptually represents the amount of time passed since the water entered the aquifer. From this an integrated groundwater flow time-rate can be estimated. However atmospheric CO_2 is typically not the only, or even a major, source of IC in most groundwater systems. A range of sources/processes including seawater infiltration, the presence of connate water, dissolution of carbonates and oxidation of organic matter can all contribute to the IC in the system. Given that each of these sources may have different radiocarbon mean residence times the apparent radiocarbon mean residence time of the bulk IC actually represents a weighted integrated age distribution of all sources rather than a single age (Bethke and Johnson, 2002; Bethke and Johnson, 2008). This means that measured mean residence time is actually a weighted average from multiple inputs rather than a single point source – this applies to both OC and IC radiocarbon mean residence times (Plummer and Glynn, 2013).

Several adjustment approaches have been developed to calculate the proportion of radiocarbon attributed to atmospheric carbon only and hence to provide an estimate of atmospheric recharge mean residence times (Plummer and Glynn, 2013). For the most part these methods work by assuming recharge carbon has been diluted with carbon from other sources. In some models, like the long established Tamers' and Pearson's models, as well as more recent models, the approach used is a simple dilution from carbonate dissolution (Ingerson and Pearson, 1964; Tamers, 1967; Pearson and Hanshaw, 1970; Tamers, 1970; Tamers and Scharpenseel, 1970; Coetsiers and Walraevens, 2009). More advanced models such as Fontes and Garnier's model use two-part mixing between the soil zone

and carbonate dissolution (Fontes and Garnier, 1979; Fontes, 1992) or between different carbonate and silicate end-members (Harrington and Herczeg, 1998). In all cases these models are using two or fewer end-members to calculate radiocarbon mean residence time since recharge.

This results in two limitations: firstly, depending on the nature of the study it may be more pertinent to work out the mean residence time of another source of IC, notably, for example, oxidation of OC, than the mean residence time of recharge (Harvey et al., 2002). Calculating the mean residence time of IC derived from the oxidation of OC is important because the oxidation of OC is involved in redox reactions which control the mobility of many contaminants in groundwaters (*i.e.* Fe, As, Mn, U *e.g.* Islam et al., 2004; Newsome et al., 2017). For example, several studies have used the radiocarbon mean residence time of IC to trace OC driven inorganic contamination and these also often use $\delta^{13}C$ has a complementary stable isotopic technique to trace the origins of carbon (Harvey et al., 2002; Lawson et al., 2013; Lawson et al., 2016).

Secondly, the processes controlling groundwater chemistry are often inherently more complex than simple two-part mixing and this limits the utility of existing models. Coetsiers and Walraevens (2009) demonstrated how assuming the stoichiometry of OC oxidation processes can be used to provide a radiocarbon adjustment in carbonate dominated aquifers. Isotopic balancing approaches have been successfully applied in two-part systems. Fontes and Garnier (1979)'s hugely influential model uses carbon isotopes to provide a correction from soil zone influxes and carbonate dissolution whilst Harrington and Herczeg (1998) demonstrated the application of the $^{87}Sr/^{86}Sr$ ratio to constrain radiocarbon mean residence times between silicates and carbonates. But currently few high-profile models have been able to provide radiocarbon adjustments in aquifers with complex mineralogy with end-member substitution (Plummer and Glynn, 2013).

The $^{87}Sr/^{86}Sr$ in combination with cationic ratios has been used to quantify weathering fluxes in rivers running through catchments with multiple water-rock reaction derived end-members. For example, $^{87}Sr/^{86}Sr$ has been used to study rock weathering as evidenced by circum-Himalayan rivers (Jacobson and Blum, 2000; Bickle et al., 2001; Bickle et al., 2003; Oliver et al., 2003; Bickle et al., 2005; Colin et al., 2006; Tipper et al., 2006a; Tipper et al., 2006b; Liu et al., 2007; Jin et al., 2011), the Congo (Négrel et al., 1993), the Amazon (Allègre et al., 1996) and in central Europe (Négrel and Deschamps, 1996; Négrel et al., 1997; Négrel, 1999). In groundwater studies similar approaches have been used in aquifers across the global. Studies include surface-water-groundwater interaction (Harrington et al., 2002; Négrel and Petelet-Giraud, 2005), saline intrusion (Cartwright et al., 2007; Ettayfi et al., 2012), groundwater evolution in silicate dominated aquifers (Harrington and Herczeg, 2003; Cartwright, 2010) and groundwater evolution in carbonate dominated aquifers where the strontium isotopic

147 approach have been compared to bulk radiocarbon mean residence times (Dogramaci and Herczeg,
148 2002; Li et al., 2010). Here we combine the approach of multi-end-member $^{87}Sr/^{86}Sr$ mixing models
149 with assumptions on the stoichiometry of IC generating reactions to provide a new approach to
150 radiocarbon adjustment that will calculate the model mean residence time of IC formed from the
151 oxidation of OC.

152 The aim of this study, therefore, is (i) to develop a new radiocarbon adjustment technique which can
153 be used to estimate the mean residence time of organic sourced inorganic carbon (i.e. inorganic
154 carbon which is formed by the oxidation of organic material, we refer to this as OrCSIC hereafter) and
155 (ii) to demonstrate its application in a case study of a mixed silicate-carbonate aquifer. This is a new
156 approach to radiocarbon adjustment and allows for the improved understanding of the physical and
157 geochemical history of aquifers in a number of settings.

158 # 2) Methodology

159 ## 2.1 Outline of new approach

160 In the present study, a method is proposed to calculate both the concentration and the radiocarbon
161 mean residence time of OrCSIC (organic carbon sourced inorganic carbon). The full method is provided
162 in Appendix A with an overview provided here. The method assumes the groundwater has four IC end-
163 members. The first is the dependant end-member, OrCSIC, and the rest are independent end-
164 members which will vary based on local conditions. Dependant end-members include water based
165 end-members such as rainwater via recharge (i.e. carbonate from soil zone), seawater, connate water
166 and end-members based on water-rock interaction (e.g. silicate-weathering derived groundwater,
167 carbonate-weathering derived groundwater *etc.*).

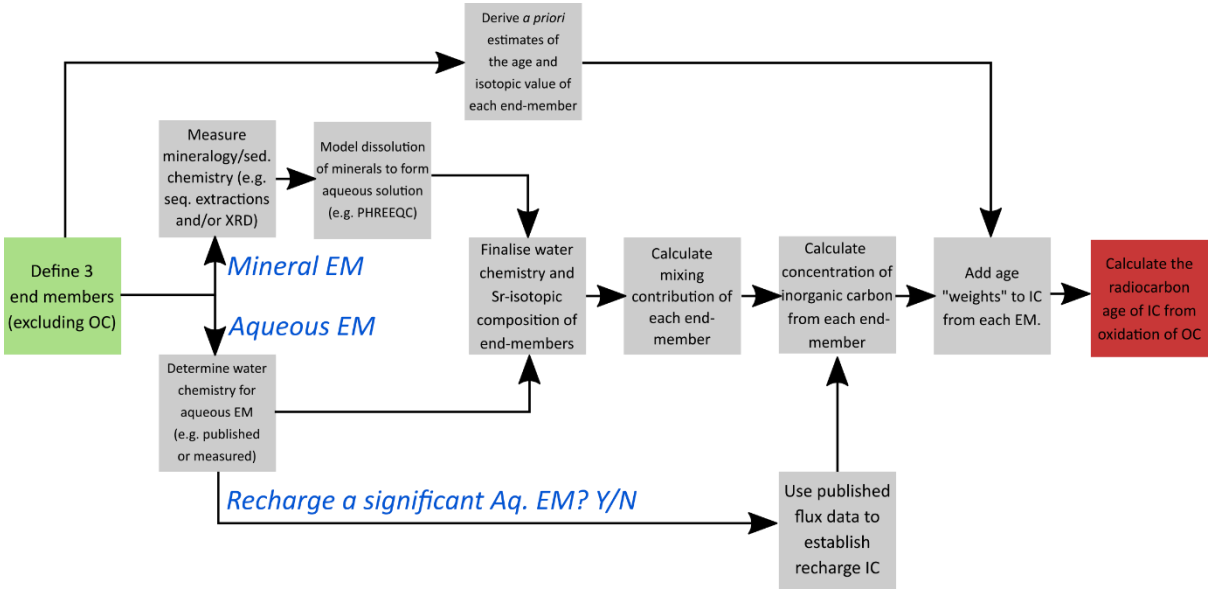

Figure 1 Flow chart of the approach outlined in this study. N.B. EM refers to end-member; IC refers inorganic carbon.

The independent end-members must be well defined with respect to both $^{87}Sr/^{86}Sr$ and the chemical tracers (e.g. in this example, Ca/Na and Mg/Na). In addition, each have known or approximated mean residence times for example a carbonate end-member produced entirely from rocks older than 60 kyr can be assumed to have $\Delta^{14}C$ of -1000 ‰ whilst and end-member exclusively from recharge from the 1960s will have a value of between 600 and 900 ‰ depending on latitude. For water end-members, this simply represents the direct concentration of a representative sample (e.g. seawater chemistry) and approximate ages. For mineralogical end-members (e.g. an assemblage of carbonate or silicate minerals) a representative mineralogical sample must first be produced and this is then converted to a water end-member by assuming the dissolution solely of these minerals into de-ionised water. Chemically, this conversion is best achieved through geochemical modelling (e.g. PHREEQC). It is assumed that there is no fractionation of the $^{87}Sr/^{86}Sr$ ratio during mineral dissolution and that there is subsequent conservative mixing of the chemical tracers selected. The equations used quantify the model by calculating (i) contributions of each end-member to groundwater using $^{87}Sr/^{86}Sr$, Ca/Na and Mg/Na; (ii) the contributions of each end-member to groundwater IC stoichiometrically; (iii) the contributions of IC derived from the oxidation of OC (OrCSIC) by subtraction of these from the bulk; (iv) the model ^{14}C of OrCSIC by from the weighted average of each end-member ^{14}C and its relative contribution (Figure 1).

2.2 Case Study - Locality, sample collection and groundwater measurements

The case study site is an inland location in northern Kandal Province, Cambodia about 10 km south of the capital Phnom Penh. The area is located between two rivers, the major Himalayan river, the Mekong, and its distributary, the Bassac, with wetlands seasonally present in the central area (Figure 2A). The groundwater here is mostly Ca-HCO_3 type with evidence of mixing with Na-Cl type waters but with no evidence of substantial cation exchange (Appelo and Postma, 2005; Richards et al., 2017a). This suggests that the model assumption of conservative mixing is valid for this site.

The site contains some of the highest concentrations of groundwater arsenic in Cambodia (Sovann and Polya, 2014) and which is widely acknowledged to be caused by reductive dissolution of iron-oxide minerals associated with OC oxidation (Rowland et al., 2007). Our study site is divided into two transects the first being a predominantly sandy transect running parallel to groundwater flow and perpendicular to the Bassac River for about 4.5 km (T-Sand) and another transect (also parallel to groundwater flow) is about 6 km due west, extending for 3 km from the Mekong with mixed sand and clay sediments (T-Clay, Figure 2A). In addition to our own transects, we also provide the location of and data from an additional transect (T-Flow, Figure 2A) where groundwater flow has been modelled by other researchers (Benner et al., 2008; Kocar et al., 2008; Polizzotto et al., 2008).

A complete description of these transects are provided elsewhere (Benner et al., 2008; Magnone et al., 2017; Richards et al., 2017a; Uhlemann et al., 2017; Richards et al., 2018) but in short, T-Sand consists of mid-Holocene (2 kyr – 4 kyr) sand-sized sediments from 9 m to 30 m or >45 m which are capped with more recent clays (<1.6 kyr) sized sediments to a depth of approximately 6 to 9 m. The broadly layer cake structure of T-Sand is typical of much of the sediments in the region with the shallow clay cap also existing extensively in the area (Magnone et al., 2017). Like T-Sand, T-Flow also has a layer cake structure with clay overlying a sandy aquifer (Figure 2B) (Benner et al., 2008). However, in contrast, T-Clay does not have this structure and consists of mostly clay-sized sediments down to 30 m with some sandy variably continuous layers ; most of T-Clay's sediments were deposited in the early Holocene (>6 kyr) (Magnone et al., 2017).

On T-Flow, net groundwater flow throughout the year is from the wetlands to the rivers however the there is a distinctive seasonal groundwater flow pattern (Figure 2B). Following the rainy season flow is from the river to the wetlands however at the peak of the dry season flow reverses and is from the wetlands to the river. Water flows vertically down through the clay layer and horizontally through the sand before reaching the river (Benner et al., 2008). Similarities between T-Sand & T-Clay and T-Flow

in seasonal fluctuations in groundwater levels indicate that similar flow patterns exist across the study site (Richards et al., 2017a).

The flow modelling of T-flow indicates that if water recharges 3500 m from the river (i.e. near the wetlands) via the clay layer it will take nearly 900 years to reach the river. If water recharges 670 m from the river but still via the clay layer it will take about 320 years to reach the river (Figure 2B). In both cases between 250 and 285 years are spent flowing the short distance through the clay layer with the remaining time spent flowing much further through the sandy aquifer (Benner et al., 2008). Tritium and CFC dating from T-Sand and T-Clay indicates that much of the recharge is <50 years old (Lawson et al., 2013; Lawson et al., 2016; Richards et al., 2016; Richards et al., 2017b; Richards et al., 2019c). These values are substantially shorted than suggested by the flow modelling (Benner et al., 2008) and indicate that recharge may be via clay windows rather than via the clay layer (Lawson et al., 2013; Lawson et al., 2016; Richards et al., 2016; Richards et al., 2017b; Richards et al., 2019c).

Such flow patterns are important to the chemistry as there is some debate as to whether key redox processes occur predominantly in the shallow clay sediments (Benner et al., 2008; Kocar et al., 2008; Polizzotto et al., 2008; Stuckey et al., 2015b) or deeper in the aquifer (Rowland et al., 2007; Lawson et al., 2013; Lawson et al., 2016; Magnone et al., 2017; Richards et al., 2018; Richards et al., 2019c). Given redox controls on arsenic mobilisation, understanding these processes is important given the context of the site. Mapping the location and mean residence times of OrCSIC will help in understanding these processes further.

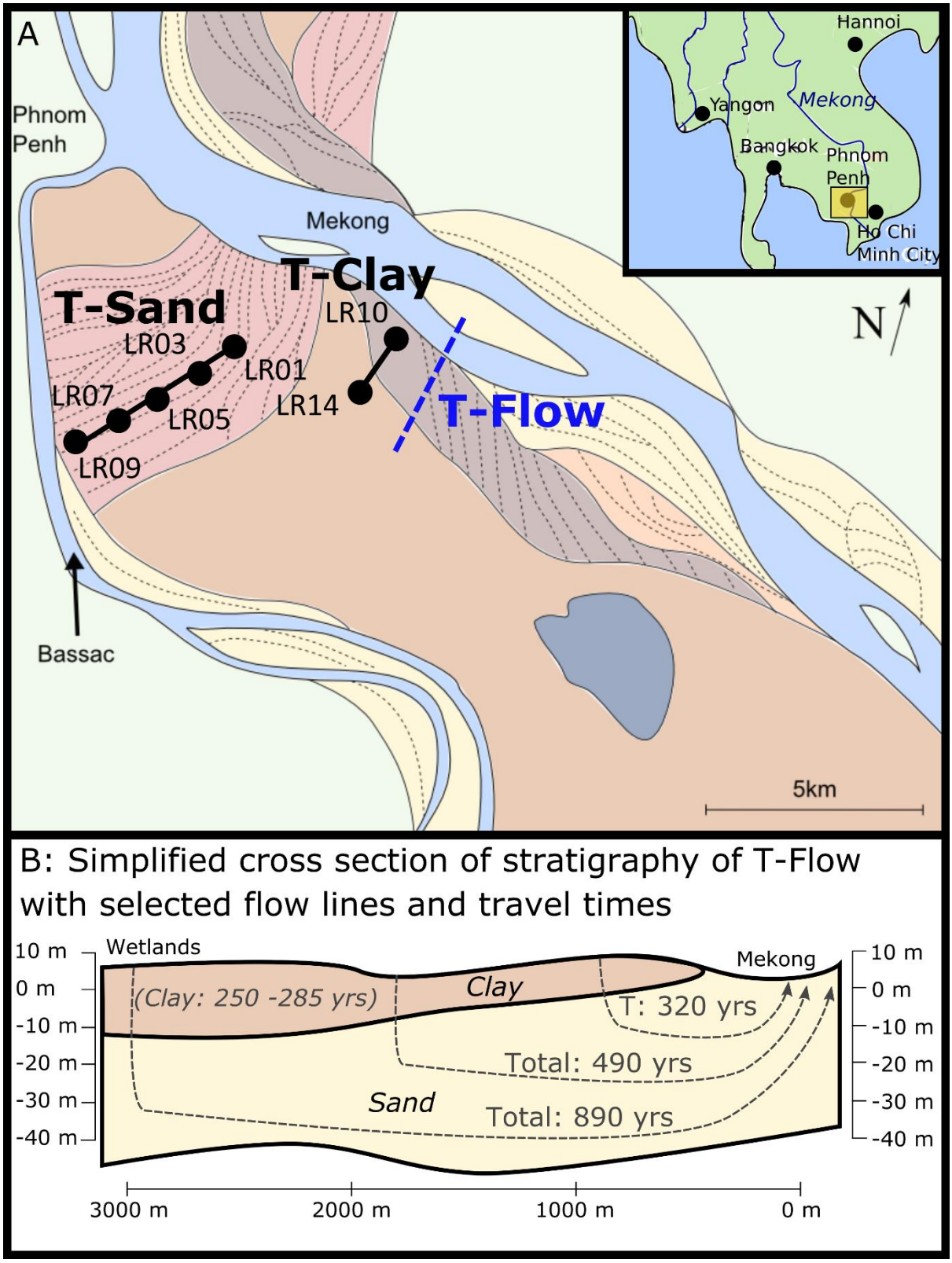

Figure 2A Map of regional setting, study area, transects and borehole sites (adapted from an original map produced by Magnone et al., (2017) reproduced under the terms of an open-access Creative Commons Attribution 4.0 International License, details of which may be found at http://creativecommons.org/licenses/by/4.0/); B Simplified stratigraphic cross section of T-Flow with selected flow lines demonstrating groundwater flow modelled travel times. "Total" indicates time from

recharge to river and "Clay" indicates flow time through clay cap. Figure is re-drawn and adapted from original data, groundwater flow modelling and cross sections from Benner et al., (2008).

2.3 Case Study - Analytical techniques

Descriptions of sampling methods have been published previously, (Richards et al., 2015; Richards et al., 2017a; Richards et al., 2019c) with details of new analytical methods used for this study outlined below. Samples were collected in both the pre-monsoon and post-monsoon seasons, however only the pre-monsoon ^{14}C data are used here (NRCF allocation 1835.0714). Post-monsoon and further pre-monsoon radiocarbon data were also obtained from a further allocation, NRCF 1906.0415, but are excluded from this study because of concerns over the stability of radiocarbon and stable carbon isotopic compositions during prolonged storage prior to sample preparation. Water samples for $^{87}Sr/^{86}Sr$ and cation analysis were filtered through 0.45 µm cellulose and polypropylene syringe filters (Minisart RC, UK) and acidified in the field to pH <2 with nitric acid (Trace grade nitric acid, BDH Aristar, UK). A volume of 2.5 L was collected for ^{14}C OC analysis. All the above samples were stored refrigerated after collection. For ^{14}C IC analysis, water (500 mL) was collected in 1L FlexFoil Plus bags, which had been pre-flushed with nitrogen at the University of Manchester, and then stored frozen (~ -20 ^{o}C) before analysis (Bryant et al., 2013). Sample are named in the form LRXX-#-PRE, where LRXX refers to the site, # to the depth in meters and PRE refers to the season of collection.

Analytical bulk water chemistry techniques and results for these samples have been published elsewhere (Polya et al., 2017; Richards et al., 2017a); where additional data are provided in this study, further information is provided here. Alkalinity (reported as HCO_3^- equivalent) was measured in the field using a field titration kit (Aquamerck 111109, Merck, Germany) and corroborated for selected samples using a Gran Titration method within 24 hours (Richards et al., 2017a). H_2CO_3 was calculated from measured pH and the known acid dissociation constant of carbonic acid, ($K = 10^{-6.35}$) for both groundwater and rainwater samples using Equation 2 (Appelo and Postma, 2005).

Equation 2

$$H_2CO_3 = \frac{10^{-pH} \cdot HCO_3-}{K_1}$$

Strontium isotopic ratios were measured at the NERC Isotope Geosciences Laboratory. Samples were opened in a clean laboratory (class 100, laminar flow) and 10 ml of each sample was transferred into a pre-cleaned Teflon beaker. Samples were dried down in chloride form using 6M HCl. Residues were taken up in 2.5M HCl and strontium was collected using Eichrom AG50W X8 resin columns. Strontium was loaded onto a single Re Filament following the method of Birck (1986). The isotope composition

was determined by Thermal Ionisation Mass Spectroscopy (TIMS) using a Thermo Triton multi-collector mass spectrometer. The international standard for $^{87}Sr/^{86}Sr$, NIST987, gave a value of 0.710257 ±0.000016 (n=43, 2SD) during the analysis of these samples.

All water samples for radiocarbon analysis were prepared as graphite (Slota et al., 1987) at the NERC Radiocarbon Facility (East Kilbride, UK) and analysed on the SUERC AMS (Xu et al., 2004; Freeman et al., 2008). All $\delta^{13}C$ values were measured using a dual inlet stable isotope mass spectrometer (Thermo Fisher Delta V) and are reported relative to the Vienna Pee Dee Belemnite (VPDB) (Coplen, 1994). Samples for ^{14}C of OC were treated by rotary evaporating an aliquot of the sample down to a few millilitres before quantitative transfer to pre-weighed acid washed beakers. Samples were covered with glass fibre filters and freeze-dried before placing in a desiccant free glass desiccator with a beaker of concentrated hydrochloric acid in order to hydrolyse any inorganic carbon present. The desiccator was placed in a water bath at 67 ^{o}C (making the internal temperature of the desiccator 63 ± 2 ^{o}C) and the air evacuated using a vacuum pump. Total carbon was recovered as CO_2, which was cryogenically isolated and graphitised with Fe/Zn reduction (Slota et al., 1987). ^{14}C IC samples were prepared from defrosted samples by liberating carbon as CO_2 using hydrolysis by H_3PO_4. All radiocarbon is reported in the conventional form of $\Delta^{14}C$ (Stuiver and Polach, 1977).

2.4 Case Study – Determining end-members values

2.4.1 $^{87}Sr/^{86}Sr$ and chemistry of end-members

Three independent end-members were selected: direct recharge reacting with silicate (EM-silicate); direct recharge reacting with carbonate minerals (EM-carbonate); minerals and recharge via the soil zone (EM-recharge). For clarity: EM-silicate is a water whose chemistry is entirely formed by reactions with silicate mineral assemblages which exist in the local area; EM-carbonate is a water whose chemistry is entirely formed by reactions with carbonate mineral assemblages which exist in the local area; and EM-recharge is defined rainwater which has recharged to the aquifer via the soil zone.

At the study site, the dominant silicate minerals are montmorillonite, albite, phlogopite and muscovite (Rowland et al., 2007; Stuckey et al., 2015a) whilst upstream in the catchment, outcrops of karstic limestones exist providing a source of carbonate minerals (Gupta, 2009; Kiernan, 2009; Ponta and Aharon, 2014). Karstic limestones are dominated mineralogically by calcite ($CaCO_3$) and dolomite ($CaMg(CO_3)_2$) with Sr and Na as common impurities (Ford and Williams, 2013). The site is not located near the coast and has rapid recharge rates suggesting that no other end-member (e.g. seawater, connate waters) is important (Benner et al., 2008; Polizzotto et al., 2008; Lawson et al., 2013; Lawson et al., 2016; Richards et al., 2017b; Richards et al., 2019c).

To derive the mineralogical end-members sequential extractions of sediments were undertaken (described at 2.4.2) to obtain the elemental and isotopic composition of the carbonate and silicate fractions of sediments (e.g. $^{87}Sr/^{86}Sr$, Ca, Mg, Na, Sr) (Jacobson and Blum, 2000; Mossop and Davidson, 2003; Colin et al., 2006; Liu et al., 2007; Kamenov et al., 2009). Sediment samples were selected (LR01-6, LR05-6, LR09-6, LR09-30 and LR14-30) to represent a selected sub-range of localities, depths and chemical compositions from across the study area (Magnone et al., 2017; Richards et al., 2017a; Richards et al., 2019a). Samples were oven dried to remove any moisture and heated to 550 ^{o}C to remove any OC. The carbonate phases were extracted with 5M glacial acetic acid (CH_3OOH, ≥99.85%, Sigma Aldrich) at approximately 25 ^{o}C for 24 hours, the sample was centrifuged and the supernatant removed stored for further analysis. The iron oxide phases were removed using 5 % (w/w) analysis grade hydrochloric acid (HCl 37%, Certified AR for Analysis, Fisher Scientific) this was removed, stored and analysed but the results are not used in this study as they are not required for three-part mixing. The silicate phases were digested with 2 ml 18.2M Ω Milli-Q water, 2 mls ultrapure concentrated HCl and 6 ml concentrated hydrofluoric acid (HF). Samples were placed in a microwave (MARS 5 Xpress: CEM corp) for 55 mins at 170 °C, left to cool and microwaved repeatedly until complete dissolution (this ranged from twice to eight times). Samples were evaporated to incipient dryness before being re-dissolved in 2% hydrochloric acid for analysis.

The mineral assemblages for both mineralogical end-members were built based on the minerals stated above. The abundance of each mineral was calculated to be consistent with the sequential extraction data (see Appendix A for calculations). PHREEQC was used to calculate the hydrological end-member and the full code is provided in Appendix A. The keyword REACTION was used to stepwise add minerals to a solution of de-ionised water starting at pH 4.6 with each step into dependent upon the solution composition or time. This assumed a steady state equilibrium system without any other chemical effects (Parkhurst and Appelo, 2013), in particular we assume no exchange processes due to the low CEC in the area (Hengl et al., 2014; Hengl et al., 2017) and negligible redox effects due to the low reduction potentials of Ca, Mg and Na. This approach was chosen to determine a hypothetical end-member prior which was solely controlled by the mineral composition of the sediments partial dissolution of which it was derived. The reactions were charge balanced with potassium, which was selected as the model calculations are insensitive to its concentration .

The reaction was stopped and end-member solution determined when either: 1) all minerals became saturated; 2) if minerals never became saturated then at peak Ca/Na and Mg/Na – which ever came later; 3) if Ca/Na and Mg/Na never peaked then at the point of plateauing – which ever came later. This approach was selected to ensure that the end-members were determined independently of the

groundwater chemistry – preventing researcher driven bias – and ensuring that the values represented a solution with chemistry was entirely dictated by the bulk mineral chemistry.

Recharge is assumed to be the rainwater chemical composition with negligible cation exchange due to the low cation exchange capacity of soils in the region (<50 cmolc/kg) (Hengl et al., 2017). Whilst this is a major simplification it provides the purest end-member thus constraining sites with minimal equilibration in an area of rapid recharge. Rainwater chemistry was determined from the World Data Center for Precipitation Chemistry (WDCPC). For Ca and Mg mean concentration and standards errors were calculated from data for stations in Thailand and Malaysia collected between 1996 – 2016 and 1987 – 2016 respectively (WDCPC, 2016), with an inverse distance weighted mean used as the value for rainwater at the study site. The WDCPC data were preferred to a single rainwater sample collected by this project because they are collected over several decades rather than a single rainy season and thus is representative of long-term atmospheric recharge. The strontium isotopic composition was measured by this project from a sample collected from a seasonal cumulative rainwater sample tank but was verified by comparison to other strontium isotopic values of rainwater in South East Asia (Nakano and Tanaka, 1997; Bentley, 2006; Xu and Han, 2009; Cheng et al., 2010; Han et al., 2011; Chatterjee and Singh, 2012) and against modern seawater values from which most deltaic rainwater could be expected to be derived (Drever, 1997; McArthur et al., 2001; Bickle et al., 2003; Oliver et al., 2003). As detailed in the results the value was very close to modern seawater and other circum-Himalayan rainwaters indicating it is a reliable value. Thus, the most important difference between EM-recharge and rainwater is the addition of CO_2 from root respiration which is accounted for with globally published fluxes (Kessler and Harvey, 2001).

2.4.2 Radiocarbon mean residence times and δ13C of end-members

Each of the end-members (EM-carbonate, EM-silicate and EM-recharge) require approximations of $\Delta^{14}C$ and $\delta^{13}C$ to calculate the value for oxidised OC. Any recent carbonate dissolution is accounted for within the recharge end-member. Carbonate and silicate end-members represent the in-aquifer dissolution of geologically sourced minerals. For these we use the $\Delta^{14}C$ and $\delta^{13}C$ values provided by Geyh (2000) calculated using Vogel's reservoir adjustment technique (Vogel, 1970), viz. crystalline rock (used for EM-silicate) have values of about $\Delta^{14}C$ = 0 ‰ for crystalline rocks (silicates) 0 ‰ and $\Delta^{14}C$ = -350 ‰ for limestone karsts (used for EM-carbonate) (Geyh, 2000). Due to the rapid rates of recharge and the bomb-carbon peak the recharge end-member is more complex. However tritium and CFC dating by earlier studies (Richards et al., 2017b; Richards et al., 2019c) and groundwater flow modelling (Benner et al., 2008) indicates four key ages of recharge; recent (2014 – 2005), post-peak (2005 – 1990), peak (1990 – 1965) and pre-bomb (1965 – 1915). These correspond to radiocarbon

mean residence times of $\Delta^{14}C$ values of 50, 150, 700 and 0 ‰ respectively (Hua et al., 2013). For $\delta^{13}C$ we assume both recharge and silicate to have values -14 ‰. This assumes C3 plants as the dominant source, these have $\delta^{13}C$ of -27 ‰ however diffusion of CO_2 in the soil zone enriches this by +4.4 ‰ and the dissolution of CO_2 to HCO_3^- enriches by +9 ‰ due to fractionation. Carbonates are assumed to have a $\delta^{13}C$ of -7 ‰. In an open system, CO_2 from dissolved carbonate have a value of -16 ‰, however, this also enriches by +9 ‰ during dissolution to HCO_3^- making it -7 ‰ (Appelo and Postma, 2005). These values are presented in Table 1.

Table 1 A priori end-members for carbon isotopes for inorganic carbon. N.B. Diffusive and fractionation processes have been accounted for (Deines, 1980; Geyh, 2000; Appelo and Postma, 2005; Hua et al., 2013).

End-member	**Bomb ^{14}C Present**	**$\delta^{13}C_{IC}$ ‰**	**$\Delta^{14}C_{IC}$ ‰**
Rainwater	Pre-1950	-14	0
	Peak		700
	Post-peak		150
	Recent		50
Silicate	N/A	-14	0
Carbonate	N/A	-7	-350

2.4.3 Proportions of each end-member and IC proportioning

Once $^{87}Sr/^{86}Sr$ and Ca, Mg, Na and Sr end-member values were established using the method in 2.4.1 the relative contribution of each end-member to the solutes in the groundwater was calculated using equations provided in Appendix A. All calculations were undertaken in R with code provided in Appendix B and description of use provided in Appendix C. Once the proportion of each end-member was calculated the proportion of IC from each end-member was calculated based on stoichiometric assumptions (see appendix for details). Any IC not from an end-member was assumed to be OrCSIC. To calculate the $\Delta^{14}C$ and $\delta^{13}C$ of OrCSIC a weighted average of each end-member IC concentration and its $\Delta^{14}C$ and $\delta^{13}C$ (Table 1) was subtracted from total IC concentration and $\Delta^{14}C$ and $\delta^{13}C$ with the full equations provided in the Appendix A.

3) Results

3.1 Groundwater chemical composition and measured radiocarbon values

The pH of these groundwaters was circum-neutral, ranging from 6.6 to 7.5 with a mean (± st. dev.) of 7.0 ± 0.3 (Table 2). IC (the sum of the inorganic carbonate species) ranges from 4.4 mM to 18.9 mM, with a mean of 7.9 ± 4.1 mM. Due to the near neutral pHs, most of the IC is dominated by HCO_3^- which comprises of 67 to 94 % of total IC (Table 2). The most dominant of the geologically sourced components (*i.e.* no organic component only mineralogical and rainwater: Ca, Na and Mg) are Na (range 0.30 to 4.2 mM; mean 1.5 ± 1.1 mM, n = 24), Ca (range 0.80 to 3.0 mM; mean 1.8 ± 0.6 mM, n = 24) andMg (range 0.50 to 2.1 mM; mean 1.0 ± 0.4 mM, n = 24, Table 2). Ca/Na ranges from 0.4 to 5.0 (mM/mM) whilst Mg/Na ranges from 0.2 to 2.8. Mean Ca/Na ratios are higher than the Mg/Na ratios (p = 0.006) with means of 1.8 ± 1.2 (mM/mM) and 0.99 ± 0.6 (mM/mM) respectively (n=24). T-Sand has higher Ca/Na and Mg/Na ratios than T-Clay (p = 0.02 for both).

Strontium concentrations range from 2.20 µM to 7.40 µM with a mean of 4.4 ± 1.5 µM (n = 24). T-Sand has statistically higher concentrations than T-Clay (p = 0.02) with means of 5.5 ± 1.5 µM and 3.9 ± 1.2 µM, respectively. Isotopically the $^{87}Sr/^{86}Sr$ of samples range from 0.71055 to 0.71250 with a mean of 0.71126 ± 0.00047 (n = 23), there is no statistically significant difference between the strontium isotopic values in T-Sand and T-Clay (p = 0.55; Table 2). The ^{86}Sr concentration is assumed to be 9.86 % of the total strontium concentration (de Laeter et al., 2003).

Table 2 Selected geochemical parameters of the groundwater of Kandal Province, Cambodia required for calculations (all data from Richards et al., (2017a) *except $^{87}Sr/^{86}Sr$ and carbonate speciation calculations which were conducted by this study). For complete data readers should refer to* Richards et al., (2017a).

Sample ID[a]	pH	HCO_3- (mM)	H_2CO_3 (mM)	Ca (mM)	Mg (mM)	Na (mM)	Sr (µM)	$^{87}Sr/^{86}Sr$ (± 0.00005)
LR01-6-PRE	6.9	5.1	1.28	1.9 ± NA	1.4 ± NA	0.5 ± NA	4.3 ± NA	0.71142
LR01-9-PRE	6.8	3.4	1.08	1.4 ± 0.1	0.7 ± 0.1	0.5 ± 0.1	2.3 ± 0.8	0.71065
LR01-15-PRE	7.0	3.7	0.74	1.1 ± 0.2	0.6 ± 0.2	0.9 ± 0.2	2.9 ± 0.8	0.71168
LR01-30-PRE	7.2	4.5	0.57	1.1 ± 0.1	0.5 ± 0.1	1.4 ± 0.1	4.3 ± 1.1	0.71113
LR01-45-PRE	6.9	3.6	0.90	1.1 ± 0.1	0.6 ± 0.1	0.5 ± 0.1	2.2 ± 0.3	0.71109
LR02-15-PRE	7.1	3.8	0.60	1.3 ± 0.1	0.5 ± 0.0	0.7 ± 0.1	3.9 ± 1.0	0.71141

LR02-30-PRE	6.6	3.0	1.50	2.4 ± 0.1	0.8 ± 0.0	0.7 ± 0.0	3.0 ± 1.0	0.71144
LR05-6-PRE	6.8	3.8	1.20	1.5 ± 0.1	0.5 ± 0.1	0.3 ± 0.0	2.8 ± 0.8	0.71149
LR05-15-PRE	7.1	5.1	0.81	1.2 ± 0.1	0.8 ± 0.2	0.9 ± 0.2	4.4 ± 1.9	0.71146
LR05-30-PRE	6.6	4.0	2.00	1.7 ± 0.3	1.0 ± 0.2	0.7 ± 0.2	3.8 ± 0.6	0.71098
LR07-15-PRE	7.1	4.5	0.71	1.5 ± 0.1	0.9 ± 0.1	0.5 ± 0.1	3.5 ± 0.8	0.71107
LR07-30-PRE	6.9	7.0	1.76	2.6 ± 0.5	1.9 ± 0.5	1.1 ± 0.3	4.5 ± 1.5	n.d.
LR09-6-PRE	6.8	13.2	4.17	3.0 ± 0.3	2.1 ± 0.3	1.6 ± 0.2	7.0 ± 1.6	0.71155
LR09-9-PRE	7.2	5.6	0.70	1.6 ± 0.1	0.8 ± 0.1	0.8 ± 0.1	5.2 ± 1.6	0.71085
LR09-30-PRE	7.2	5.4	0.68	0.8 ± 0.2	0.9 ± 0.3	2.1 ± 0.5	3.6 ± 0.8	0.71056
LR09-45-PRE	7.1	8.5	1.35	1.8 ± 0.0	1.1 ± 0.0	2.5 ± 0.0	4.1 ± 0.6	0.71124
LR10-9-PRE	7.0	9.0	1.80	2.9 ± 0.6	1.9 ± 0.6	3.0 ± 0.9	5.6 ± 1.8	0.71100
LR10-15-PRE	7.5	8.6	0.54	1.8 ± 0.0	0.8 ± 0.0	2.3 ± 0.0	7.2 ± 2.5	0.71099
LR10-21-PRE	7.5	7.6	0.48	2.0 ± 0.2	0.8 ± 0.1	2.1 ± 0.2	7.4 ± 2.4	0.71055
LR10-30-PRE	7.0	6.8	1.36	1.9 ± 0.1	1.1 ± 0.0	3.8 ± 0.2	3.2 ± 1.6	0.71224
LR14-6-PRE	6.6	10.0	5.01	2.1 ± 0.2	1.0 ± 0.2	4.2 ± 0.8	4.9 ± 1.2	0.71135
LR14-15-PRE	6.6	12.6	6.31	2.1 ± 0.5	1.1 ± 0.4	1.9 ± 0.6	6.1 ± 1.1	0.71135
LR14-21-PRE	6.8	7.9	2.50	1.7 ± 0.3	1.2 ± 0.3	1.6 ± 0.3	5.4 ± 1.7	0.71088
LR14-30-PRE	6.8	4.1	1.30	2.5 ± 0.3	1.3 ± 0.1	0.8 ± 0.0	3.8 ± 0.7	0.71250

[a] *Sample identification LRXX-#-PRE where XX denotes the site, # denotes the depth and PRE denotes these are all pre-monsoon samples* (Richards et al., 2017a).

n.d. = no data.

IC in this groundwater has an overall mean $\Delta^{14}C$ of -87.2 ± 169 ‰ (n=19) ranging from a post-bomb carbon of +83.7 $\Delta^{14}C$ ‰ at LR01-15-PRE to -535 $\Delta^{14}C$ ‰ at LR14-30 which corresponds to an approximate mean residence time of 6150 years BP. OC ranges from post-bomb -24 ± 4.5 ‰ at LR01-30-PRE to -524 ± 2.2 ‰ at LR05-6-PRE (approximately 5960 years BP) with an overall mean of -204 ± 142 ‰ (n=14) making it significantly more depleted than the IC ($p = 0.04$;). The $\delta^{13}C$ of IC ranges from -1.60 to -20.8 ‰ with a mean value of -13.0 ± 5.9 ‰ (n = 19) whilst OC broadly covers the C3 plant range ranging from -17.6 ‰ at LR01-30-PRE to -31.3 ‰ at LR14-15-PRE with a mean of -26.4 ± 3.8 ‰

(n = 14). This means that the $\delta^{13}C$ of the OC has a significantly more depleted range than that of IC (p-value < 0.001).

Table 3 Measured Radiocarbon mean residence times of IC and OC of the groundwaters of Kandal Province, Cambodia.

Sample ID[a]	Bomb carbon status[b]	$\delta^{13}C$ ‰ ± 0.1 (IC)	$\Delta^{14}C$ ‰ (IC)	IC Radiocarbon mean residence time (years BP)	Publication code (IC)	$\delta^{13}C$ ‰ ± 0.1 (OC)	$\Delta^{14}C$ ‰ (OC)	OC Radiocarbon mean residence times (years BP)	Publication code (OC)
LR01-6-PRE	Recent	-8.40	-26.6 ± 4.27	220 ± 35	SUERC-55302	-24.1	-207 ± 3.69	1860 ± 37	SUERC-56905
LR01-9-PRE	Peak	-6.50	17.2 ± 4.47	POST 1950	SUERC-56190	-26.7	-146 ± 3.77	1270 ± 36	SUERC-57669
LR01-15-PRE	Peak	-15.8	83.7 ± 5.12	POST 1950	SUERC-55292	-30.3	-143 ± 3.78	1240 ± 36	SUERC-56895
LR01-30-PRE	Peak	-18.0	30.3 ± 4.52	POST 1950	SUERC-56184	-17.6	-26 ± 4.52	210 ± 37	SUERC-57663
LR01-45-PRE	Peak	-20.8	-186 ± 3.58	1650 ± 35	SUERC-56191	-25.3	-257 ± 3.5	2390 ± 38	SUERC-57670
LR05-6-PRE	Recent	-17.3	49.5 ± 4.84	POST 1950	SUERC-62513	n.d.	n.d.	n.d.	N/A
LR05-15-PRE	Peak	-7.80	80.2 ± 4.74	POST 1950	SUERC-55299	-31.2	-24.7 ± 4.52	200 ± 37	SUERC-56900
LR05-30-PRE	Peak	-15.9	-43.9 ± 4.47	360 ± 38	SUERC-55814	-27.0	-199 ± 3.55	1780 ± 36	SUERC-57675
LR09-6-PRE	Recent	-16.5	16.6 ± 4.46	POST 1950	SUERC-56185	-21.4	-97.4 ± 3.99	820 ± 36	SUERC-57664
LR09-9-PRE	Recent	-3.00	-29.2 ± 4.47	240 ± 37	SUERC-62519	n.d.	n.d.	n.d.	N/A
LR09-30-PRE	Peak	-11.2	-80.4 ± 4.36	670 ± 38	SUERC-55293	-27.6	-116 ± 4.11	990 ± 37	SUERC-56896

LR09-45-PRE	Peak	-20.0	-102 ± 3.94	860 ± 35	SUERC-55812	-26.2	-172 ± 3.92	1520 ± 38	SUERC-57673
LR10-9-PRE	Recent	-14.3	-4.71 ± 4.60	38 ± 37	SUERC-63012	n.d.	n.d.	n.d.	N/A
LR10-15-PRE	Recent	-18.4	-6.70 ± 4.68	54 ± 38	SUERC-55300	-27.7	-232 ± 3.58	2120 ± 38	SUERC-56903
LR10-21-PRE	Recent	-15.7	-280 ± 3.37	2640 ± 38	SUERC-57686	-23.6	-267 ± 3.22	2500 ± 35	SUERC-57690
LR10-30-PRE	Recent	-17.5	-266 ± 3.45	2480 ± 38	SUERC-55811	n.d.	n.d.	n.d.	N/A
LR14-6-PRE	Recent	-14.9	15.0 ± 4.50	POST 1950	SUERC-63015	n.d.	n.d.	n.d.	N/A
LR14-15-PRE	Pre-1950	-5.20	-389 ± 2.70	3960 ± 36	SUERC-55303	-31.3	-524 ± 2.2	5960 ± 37	SUERC-56906
LR14-30-PRE	Pre-1950	-1.60	-535 ± 2.04	6150 ± 35	SUERC-56189	-29.1	-447 ± 2.67	4760 ± 39	SUERC-57666

[a] *Sample identification LRXX-#-PRE where XX denotes the site, # denotes the depth and PRE denotes that samples were collected in the pre-monsoon season.*

[b] *Indicates whether the rainwater end-member is likely to contain bomb carbon or not; based on tritium data* (Richards et al., 2016; Richards et al., 2017b).

n.d. = no data.

N/A = not applicable.

3.2 Sediment extraction results

The $^{87}Sr/^{86}Sr$ ratio for extracted silicates ranges from 0.71954 to 0.72083 with a mean of 0.72033 ± 0.00022. The silicate $^{87}Sr/^{86}Sr$ is consistent with previous studies in the region in the Tonle Sap (Day et al., 2011) and across the Mekong (Liu et al., 2007).The mean sedimentary concentrations of Ca, Mg, K, Na and Sr are 26 ± 6.7 mmol/kg, 74 ± 25 mmol/kg, 220 ± 37 mmol/kg, 160 ± 33 mmol/kg and 350 ± 120 µmol/kg, respectively (Table 5).

Table 4 The measured sedimentary elemental concentrations (Ca, Mg, K, Na, Sr) extracted with glacial acetic acid.

Sample	Ca	Mg	K	Na	Sr	$^{87}Sr/^{86}Sr$

	(mmol/kg)	(mmol/kg)	(mmol/kg)	(mmol/kg)	(µmol/kg)	
LR01-6	71	32	9.1	3.9	80	0.71158
LR05-6	43	16	7.5	3.3	40	0.71216
LR09-6	46	16	6.6	3.1	38	0.71212
LR09-30	10	1.3	1.3	0.8	29	0.71275
LR14-30	38	17	4.7	2.2	31	0.71257
Mean ± S.E.	41 ± 9.7	16 ± 4.8	5.8 ± 1.3	2.7 ± 0.54	43 ± 9.3	0.71223 ± 0.00020

438 $^{87}Sr/^{86}Sr$ ratios for carbonates range from 0.71158 to 0.71275 with a mean of 0.71223 ± 0.00020. There
439 are no published carbonate $^{87}Sr/^{86}Sr$ in the Mekong drainage basin to the authors' knowledge. There
440 is a large statistical difference between the two concentrations ($p< 0.001$) and $^{87}Sr/^{86}Sr$ ratios ($p <0.01$)
441 for the silicate and carbonate minerals. The mean concentrations of Ca, Mg, K, Na and Sr are 41 ± 9.7
442 mmol/kg, 16 ± 4.8 mmol/kg, 5.8 ± 1.3 mmol/kg, 2.7 ± 0.54 mmol/kg and 43 ± 9.3 µmol/kg respectively
443 (Table 5).

444 *Table 5 The measured sedimentary elemental concentrations (Ca, Mg, K, Na, Sr) extracted using hydrofluoric acid.*

Sample	Ca (mmol/kg)	Mg (mmol/kg)	K (mmol/kg)	Na (mmol/kg)	Sr (µmol/kg)	$^{87}Sr/^{86}Sr$
LR01-6	40	130	320	229	720	0.72031
LR05-6	13	24	210	160	80	0.72056
LR09-6	32	114	250	170	360	0.72083
LR09-30	7.6	5.1	90	41	130	0.71954
LR14-30	39	94	230	200	440	0.72042
Mean ± S.E.	26 ± 6.7	74 ± 25	220 ± 37	160 ± 33	350 ± 120	0.72033 ± 0.00022

445 The results in Table 5 and Table 6 combined with the likely mineralogy based on XRD-measured
446 mineral assemblage at the site (Rowland et al., 2007; Stuckey et al., 2015a) and the carbonate outcrops
447 located further upstream in the catchment (Gupta, 2009; Kiernan, 2009; Ponta and Aharon, 2014)
448 indicate the following mineral assemblages. The carbonate mineral assemblage contains 57 ± 25 %

calcite, 67 ± 11 % dolomite and 6 ± 1 % Na-impurity for which, for modelling purposes, we use dawsonite as a notional Na source given it is commonly found alongside calcite and dolomite (Deer et al., 2013; Ford and Williams, 2013). The silicate mineral assemblage contains 39 ± 8 % albite, 19 ± 2 % montmorillite, 36 ± 9 % muscovite and 6 ± 6 % phlogopite. Trace amounts of $SrCO_3$ and Sr_2SiO_4 are added to the carbonate and silicate assemblages respectively to account for Sr impurities.

Table 6 Derived mineral assemblages of carbonate and silicate end-members based on previous studies using XRD (Rowland et al., 2007; Stuckey et al., 2015a) *and proportioned based on results from sequential extractions (Table 5 and Table 6) and stoichiometry.*

Carbonate				***Silicate***			
Mineral	***Formula***	***mmol/kg***	***%***	***Mineral***	***Formula***	***mmol/kg***	***%***
Calcite	$CaCO_3$	25 ± 10.8	57 ± 25	*Albite*	$NaAlSi_3O_8$	160 ± 33	39 ± 8.1
Dolomite	$MgCa(CO_3)_2$	16 ± 4.8	37 ± 11	*Montmor-Ca*	$Ca_{0.165}Mg_{0.33}Al_{1.67}Si_4O_{10}(OH)_2$	78 ± 6.7	19 ± 1.6
Dawsonite	$NaAlCO_3(OH)_2$	2.7 ± 0.54	6.2 ± 1.2	*Muscovite*	$KAl_3Si_3O_{10}(OH)_2$	146 ± 37	36 ± 9.1
Sr-Carbonate	$SrCO_3$	0.04 ± 0.01	0.09 ± 0.02	*Phlogopite*	$KMg_3AlSi_3O_{10}(OH)_2$	25 ± 25	6.0 ± 6.0
				Sr-Silicate	Sr_2SiO_4	0.04 ± 0.01	
	Total ± S.E.	43 ± 16			*Total*	430 ± 102	

Reaction of these minerals in PHREEQC combined with the rules for stopping the reaction (defined in 2.4.1) results in the calculated end-members used in the mixing calculations. For Ca, Mg, Na and Sr EM-carbonate concentrations are 1.70 ± 0.47 mM, 1.07 ± 0.23 mM, 0.36 ± 0.06 mM and 3.00 ± 0.73 µM respectively, whilst EM-silicate concentrations are 0.01 ± 0.00 mM, 0.04 ± 0.02 mM, 0.06 ± 0.03 mM and 0.13 ± 0.04 µM respectively (Table 7). In some cases, the concentrations at the end-members are lower than the groundwater concentrations which is because the end-members are calculated independently of the groundwater concentrations and because there is no way of knowing exactly how much mineral would dissolve to create the hypothetical end-member. This makes calculating the exact concentrations impossible but values should be and are within a margin of error of the measured groundwater data. What is critical for the calculations is the value of the Ca/Na and Mg/Na ratios and these are 4.74 ± 1.55 (mM/mM) and 2.98 ± 0.82 (mM/mM) respectively for carbonate and 0.08 ± 0.07

(mM/mM) and 0.62 ± 0.40 (mM/mM) respectively for silicates (Table 7). These values encompass all measured datum points indicating that the end-members as calculated provide a reliable estimate.

The rainwater sample has an $^{87}Sr/^{86}Sr$ value of 0.70929 ± 0.0005 (analytical error); which is close to that of modern seawater which is widely reported to be approximately 0.709 and which is as expected given that seawater is the primary source of strontium in rainwater (Drever, 1997; McArthur et al., 2001; Bickle et al., 2003; Oliver et al., 2003). The value is also consistent with rainwater ranges reported by a large review of strontium isotopes in different geosystems (Bentley, 2006) and with more recently recorded deltaic rainwater values from across Asia (Nakano and Tanaka, 1997; Xu and Han, 2009; Cheng et al., 2010; Han et al., 2011) including in the circum-Himalayan region (Chatterjee and Singh, 2012) – so the rainwater value is used for the recharge end-member.

Table 7 Concentration of end-member aqueous solutions used for mixing calculations. Values determined through PHREEQC modelling of mineral assemblages (Table 6)

End-Member	**Ca (mM)**	**Mg (mM)**	**Na (mM)**	**Sr (µM)**	**Ca/Na**	**Mg/Na**	**$^{87}Sr/^{86}Sr$**
*Recharge (µM)**	6.97 ± 0.34	3.72 ± 0.20	27.9 ± 1.91	0.67 ± N.D.	0.25 ± 0.02	0.13 ± 0.01	0.709290
Carbonate	1.70 ± 0.47	1.07 ± 0.23	0.36 ± 0.06	3.00 ± 0.73	4.74 ± 1.55	2.98 ± 0.82	0.71223 ± 0.00020
Silicate	0.01 ± 0.00	0.04 ± 0.02	0.06 ± 0.03	0.13 ± 0.04	0.08 ± 0.07	0.62 ± 0.40	0.72033 ± 0.00022

N.D. = no data.

N.B. Recharge units are in µM not mM.

3.3 Mixing results

For the Ca/Na mixing the compositions of almost all of the groundwater samples lie within field of compositions constrained by mixing of the end-members, with the exception of LR05-6-PRE (Figure 3A, Table 8). For the Mg/Na mixing, most compositions were also within the field of composition constrained by the mixing end-members, however some samples were not fully constrained including LR01-30, LR09-30, LR10-15, LR10-21 and LR10-30 which were within one margin of calculation error and LR14-6 which was within two error margins. Only LR01-6 however fell substantial outside of the constraints (Figure 3B, Table 8). Calculations of end-member mixing ratios using Ca/Na and Mg/Na showed relatively similar mixing ratios for the EM-silicate, EM-carbonate and EM-recharge with no statistical significance between the values ($p = 0.18$, 0.18 and 0.40 respectively, $n = 23$). Mixing ratios calculated using Ca/Na were also highly and significantly correlated with those calculated using Mg/Na

(r = 0.94, 0.87 and 0.99 respectively, all p<0.01, n = 23). The similarity in the outputs between the Ca/Na and Mg/Na based calculations further validates the assumption of conservative mixing with respect to these cations at this site. EM-recharge input ranged from 19 % (Ca/Na based) and 26 % (Mg/Na based) respectively to 76 % and 68 % respectively (mean = 52 ± 12 & 50 ± 10 % respectively, n = 21, excluding LR01-6-PRE and LR05-6-PRE). For the Ca/Na calculations the EM-silicate input ranged from 13 % to 65 % with a mean of 42 ± 13 % (n = 21) whilst for the Mg/Na calculations it ranged from 26 % to 66 % (48 ± 11 %, n = 21). EM-carbonate inputs, however, ranged from about 1 % to about 22 % for Ca/Na calculations and <1 % to 11 % for Mg/Na calculations with means of 6 ± 6 % and 3 ± 4 %.

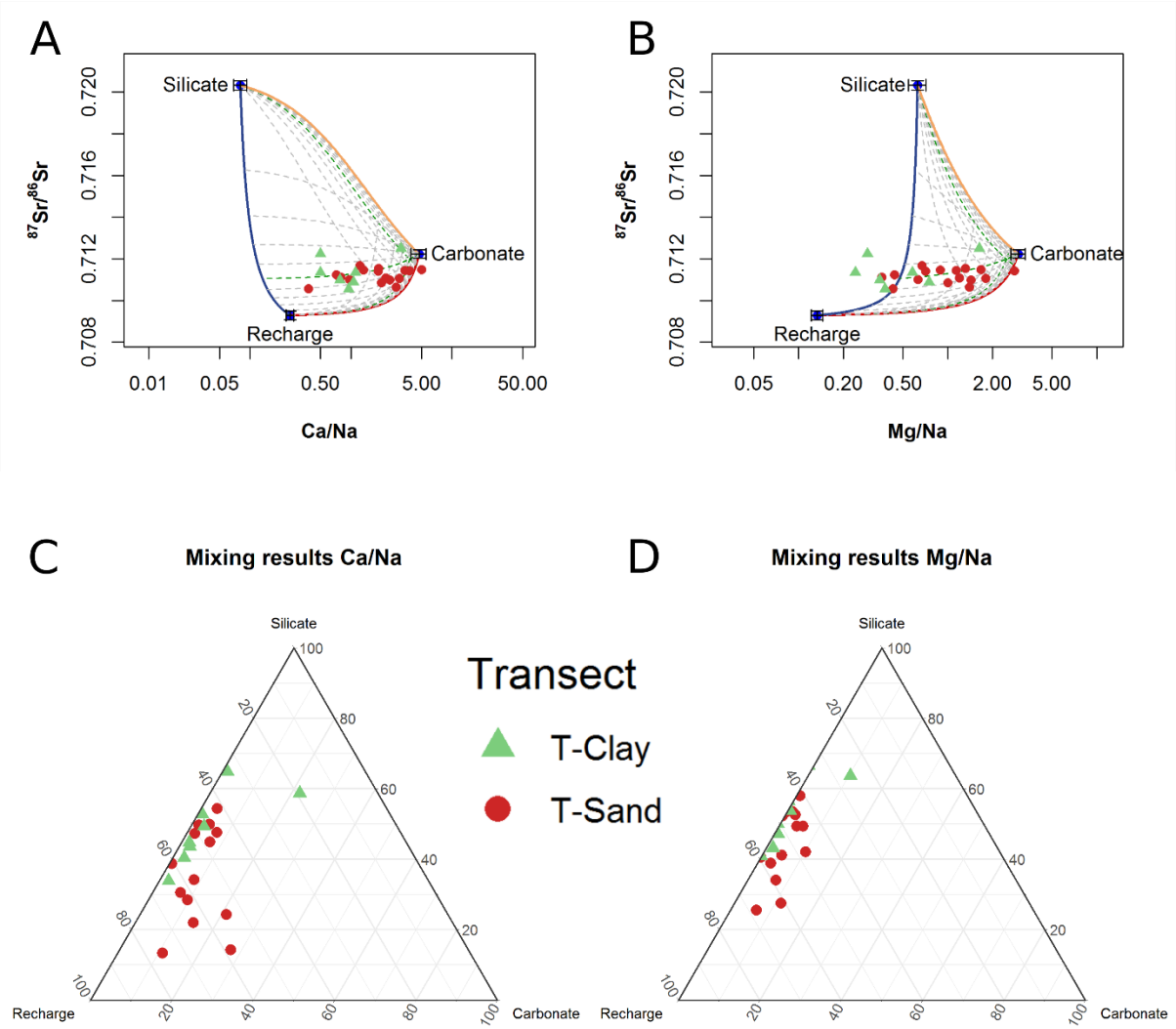

Figure 3 Groundwater composition of Kandal Province, Cambodia $^{87}Sr/^{86}Sr$ vs Ca/Na (A), $^{87}Sr/^{86}Sr$ vs Mg/Na (B) with mixing lines overlain as defined by the mixing approach of this study; Dashed lines show lines of equal end-member ratios. Results of mixing calculations illustrated in conventional ternary diagrams for $^{87}Sr/^{86}Sr$& Ca/Na (C), and $^{87}Sr/^{86}Sr$& Mg/Na (D).

Table 8 Calculated end-member(silicate, carbonate, recharge) mixing ratios (%) for groundwaters of Kandal Province, Cambodia. Based upon $^{87}Sr/^{86}Sr$ based methods utilising either Ca/Na (left) or (Mg/Na) chemical tracers.

Sample ID [a]	Ca/Na Calculations			Mg/Na Calculations		
	EM-Silicate	EM-Carbonate	EM-Recharge	EM-Silicate	EM-Carbonate	EM-Recharge
LR01-6-PRE	14 ± 19	27 ± 19	58 ± 47	-16.0 ± 19	47 ± 35	69 ± 62
LR01-9-PRE	13 ± 5.6	11 ± 7.1	76 ± 77	26 ± 7.1	6.4 ± 4.7	68 ± 52
LR01-15-PRE	54 ± 8.4	3.9 ± 2.2	42 ± 5.8	58 ± 9.2	0.9 ± 2.1	41 ± 5.5
LR01-30-PRE	47 ± 4.4	2.0 ± 0.7	51 ± 23	52 ± 7.5	-0.6 ± 0.9	48 ± 16
LR01-45-PRE	34 ± 9.0	8.4 ± 5.1	57 ± 34	41 ± 9.1	4.8 ± 4.0	54 ± 25
LR02-15-PRE	45 ± 7.6	6.9 ± 3.8	48 ± 16	54 ± 8.1	1.2 ± 2.0	45 ± 10
LR02-30-PRE	24 ± 6.0	21 ± 12	54 ± 27	49 ± 8.7	4.3 ± 3.8	46 ± 12
LR05-6-PRE	-61.2 ± 42	83 ± 57	78 ± 81	42 ± 10	10 ± 7.6	48 ± 14
LR05-15-PRE	50 ± 7.6	4.3 ± 2.3	46 ± 12	53 ± 9.1	2.4 ± 2.7	45 ± 10
LR05-30-PRE	28 ± 13	9.6 ± 6.6	62 ± 53	34 ± 11	6.9 ± 5.6	59 ± 38
LR07-15-PRE	22 ± 11	14 ± 9.2	64 ± 51	28 ± 9.0	11 ± 8.3	61 ± 37
LR09-6-PRE	48 ± 8.1	7.2 ± 4.0	45 ± 11	49 ± 9.4	5.9 ± 4.9	45 ± 9.5
LR09-9-PRE	31 ± 5.4	6.8 ± 3.8	63 ± 43	39 ± 7.7	3.2 ± 2.7	58 ± 31
LR09-30-PRE	39 ± 4.0	0.6 ± 0.2	61 ± 43	41 ± 7.3	0.0 ± 0.7	59 ± 36
LR09-45-PRE	50 ± 4.2	1.8 ± 0.5	48 ± 19	53 ± 7.6	-0.2 ± 1.1	47 ± 13
LR10-9-PRE	44 ± 6.7	2.6 ± 1.4	54 ± 27	47 ± 8.8	0.9 ± 1.6	52 ± 22
LR10-15-PRE	45 ± 4.1	1.9 ± 0.6	53 ± 28	50 ± 7.5	-0.6 ± 0.8	51 ± 20
LR10-21-PRE	34 ± 3.9	2.3 ± 0.8	64 ± 48	41 ± 7.2	-0.2 ± 0.6	59 ± 36
LR10-30-PRE	65 ± 4.3	1.3 ± 0.4	34 ± 11	66 ± 6.9	-1.3 ± 1.2	35 ± 8.4
LR14-6-PRE	53 ± 4.6	1.1 ± 0.2	46 ± 14	57 ± 7.3	-1.3 ± 0.8	45 ± 9.8
LR14-15-PRE	49 ± 8.9	3.3 ± 2.0	47 ± 15	54 ± 10	0.5 ± 1.8	46 ± 12
LR14-21-PRE	40 ± 5.6	2.8 ± 1.4	57 ± 33	43 ± 8.0	1.6 ± 1.8	55 ± 27
LR14-30-PRE	59 ± 18	22 ± 13	19 ± 38	64 ± 12	10 ± 8.2	26 ± 24

[a] *Sample identification LRXX-#-PRE where XX denotes the site, # denotes the depth and PRE denotes that these samples were all collected in the pre-monsoon season.*

511 *n.d. = no data*

512 ## 3.4 OrCSIC Calculated radiocarbon and $\delta^{13}C$ results

513 OrCSIC concentration range from below model limits at LR14-30-PRE to 14.9 ± 1.1 mM at LR14-15-PRE
514 mM (Table 9) with a mean of 4.7 ± 3.8 mM (n= 21). The OrCSIC ranges from bomb-peak carbon 170 ±
515 60 ‰ (LR01-15-PRE) to -887 ± 190 ‰ (LR10-30-PRE) with a mean of -189 ± 262 ‰. The $\delta^{13}C$ ranged
516 from -7.5 ‰ (at LR09-9-PRE) to LR01-45-PRE (at LR01-45-PRE) with a mean of 25.7 ± 9.2 ‰ (Table 9).

517 *Table 9 Calculated concentrations of IC from different geological source and that from the OC sourced IC (OrCSIC) and the*
518 *corrected mean residence times of $\Delta^{14}C$ and $\delta^{13}C$ for the groundwater of Kandal Province, Cambodia.*

	IC concentrations from difference sources (mM)				**OrCSIC isotopic values**	
Sample ID [a]	**Carbonate**	**Silicate**	**Recharge**	**OrCSIC**	**$\Delta^{14}C$ ‰**	**$\delta^{13}C$ ‰**
LR01-6-PRE	BML-M	BML-M	BML-M	BML-M	BML-M	BML-M
LR01-9-PRE	0.40 ± 0.22	0.73 ± 0.19	0.41 ± 0.04	2.94 ± 0.37	67 ± 26	-14.5 ± 0.4
LR01-15-PRE	0.10 ± 0.06	1.89 ± 0.22	0.51 ± 0.13	1.94 ± 0.34	170 ± 58	-30.2 ± 3.2
LR01-30-PRE	0.04 ± 0.02	1.56 ± 0.12	0.85 ± 0.21	2.62 ± 0.35	-163 ± 98	-34.1 ± 3.0
LR01-45-PRE	0.24 ± 0.13	1.25 ± 0.23	0.51 ± 0.13	2.50 ± 0.37	-300 ± 57	-38.3 ± 3.9
LR02-15-PRE	0.19 ± 0.10	1.70 ± 0.21	0.51 ± 0.13	2.00 ± 0.35	ND	ND
LR02-30-PRE	1.09 ± 0.60	1.96 ± 0.32	0.85 ± 0.21	0.60 ± 0.75	ND	ND
LR05-6-PRE	BML-M	BML-M	BML-M	BML-M	BML-M	BML-M
LR05-15-PRE	0.14 ± 0.08	2.04 ± 0.23	0.85 ± 0.21	2.88 ± 0.44	-24 ± 111	-13.7 ± 3.1
LR05-30-PRE	0.46 ± 0.27	1.65 ± 0.49	0.85 ± 0.21	3.04 ± 0.67	-228 ± 172	-28.9 ± 4.0
LR07-15-PRE	0.64 ± 0.35	1.16 ± 0.36	0.51 ± 0.13	2.91 ± 0.58	ND	ND
LR09-6-PRE	0.68 ± 0.38	4.93 ± 0.63	0.85 ± 0.21	10.91 ± 1.15	-6 ± 77	-29.4 ± 2.0
LR09-9-PRE	0.27 ± 0.14	1.60 ± 0.21	0.85 ± 0.21	3.58 ± 0.46	-191 ± 95	-7.5 ± 2.7
LR09-30-PRE	0.01 ± 0.02	1.35 ± 0.15	0.85 ± 0.21	3.87 ± 0.40	-279 ± 79	-21.9 ± 0.9
LR09-45-PRE	0.06 ± 0.04	2.96 ± 0.23	0.85 ± 0.21	5.98 ± 0.58	-265 ± 75	-36.0 ± 2.5
LR10-9-PRE	0.18 ± 0.12	4.32 ± 0.51	0.48 ± 0.05	5.81 ± 0.76	-1 ± 33	-26.5 ± 1.9

LR10-15-PRE	0.06 ± 0.03	2.41 ± 0.19	0.48 ± 0.05	6.19 ± 0.50	-10 ± 13	-33.4 ± 1.8
LR10-21-PRE	0.09 ± 0.03	2.01 ± 0.19	0.60 ± 0.15	5.39 ± 0.47	-432 ± 47	-29.5 ± 1.5
LR10-30-PRE	0.02 ± 0.04	3.92 ± 0.22	0.99 ± 0.25	3.22 ± 0.53	-887 ± 190	-34.6 ± 3.8
LR14-6-PRE	0.02 ± 0.02	3.35 ± 0.24	0.48 ± 0.05	11.16 ± 0.79	19 ± 10	-25.3 ± 1.1
LR14-15-PRE	0.15 ± 0.10	3.25 ± 0.44	0.60 ± 0.15	14.91 ± 1.06	-490 ± 44	-13.0 ± 0.4
LR14-21-PRE	0.13 ± 0.08	2.41 ± 0.27	0.60 ± 0.15	7.26 ± 0.61	ND	ND
LR14-30-PRE	1.37 ± 0.72	4.59 ± 0.96	0.60 ± 0.15	-1.16 ± 1.24	BML-C	BML-C

519

520 [a] *Sample identifiers are of the form LRXX-#-PRE where XX denotes the site, # denotes the depth and*
521 *PRE denotes that these are all pre-monsoon samples.*

522 *BML-M = mixing component is beyond model limits.*

523 *BML-C = modelled carbon is below model limits.*

524 *ND = no data.*

525 *NA = not applicable.*

526 ## 4) Discussion

527 This study shows that $\Delta^{14}C$ bulk IC is significantly less depleted than bulk OC whilst bulk $\delta^{13}C$ IC is
528 significantly more depleted than that of OC (Figure 4A and B, $p = 0.04$ and <0.01 respectively). This is
529 consistent with earlier studies at this (Lawson et al., 2013; Lawson et al., 2016) and other circum-
530 Himalayan sites, such as in the Indian sub-continent (Aggarwal et al., 2000; Harvey et al., 2002;
531 Dowling et al., 2003). The conventional interpretation of this observation has been that it indicates
532 that young OC is preferentially oxidised over old OC to form young IC (Harvey et al., 2002; Lawson et
533 al., 2013; Lawson et al., 2016). This interpretation, however, tacitly assumes that all IC in groundwater
534 is derived from the oxidation of OC.

535 Tracing end-member mixing with $^{87}Sr/^{86}Sr$ and the cation ratios demonstrates that this assumption is
536 not valid, indeed at this site a mean of only 57 ± 14 % of IC is from OrCSIC. Additionally, when IC from
537 EM-recharge, EM-carbonate and EM-silicate are removed from the bulk aqueous IC mean residence
538 time there is no significant difference between the of OrCSIC $\Delta^{14}C$ and aqueous OC $\Delta^{14}C$ ($p = 0.63$,
539 Figure 4A). Furthermore, excluding samples with recent recharge (*i.e.* samples that recharged
540 between 2004 and 2014, Table 2), there is a significant, almost 1:1, correlation between OC $\Delta^{14}C$ and

OrCSIC (correlation coefficient = 0.70, m = 0.96, n = 10, p = 0.02, Figure 4C). This indicates that, where recharge is not recent, OrCSIC $\Delta^{14}C$ is similar to bulk OC $\Delta^{14}C$.

The $\delta^{13}C$ of most samples were within the range of plants which have ranges of -24 to -33 ‰, -6 to -19 ‰ and -12 to -23 ‰ for C3, C4 and CAM plants respectively (Deines, 1980). Three samples, LR01-9-PRE, LR05-15-PRE and LR14-15-PRE had OrCSIC values in the C4 range whilst OC from the same locality were in the C4 range – no other pattern seems to link these samples – making it difficult to explain. More interestingly, the three sites with the lowest $\delta^{13}C$ for OrCSIC (LR01-45-PRE, LR09-45-PRE and LR10-30-PRE) are all deep sandy localities with thermally mature *n*-alkanes present in the sediments (Magnone et al., 2017) and whilst the OrCSIC $\delta^{13}C$ values are not especially depleted (-34 to -39 ‰) this may be evidence of bacterial methanotrophic processes (Whiticar, 1999). Methane has been found in the locality but the processes are only beginning to be understood however, in this case, there is no statistical association between methane concentrations and the potential methane signatures within OrCSIC (Richards et al., 2019b; Richards et al., 2019c). Adding to this, the only measured deep locality that did not have a depleted value is LR05-30-PRE and here thermally immature *n*-alkanes are present (Magnone et al., 2017). Given the sample size, the results regarding methanogenesis are certainly not conclusive but they indicate that deep aquifer methanotrophic processes should be explored further at this site.

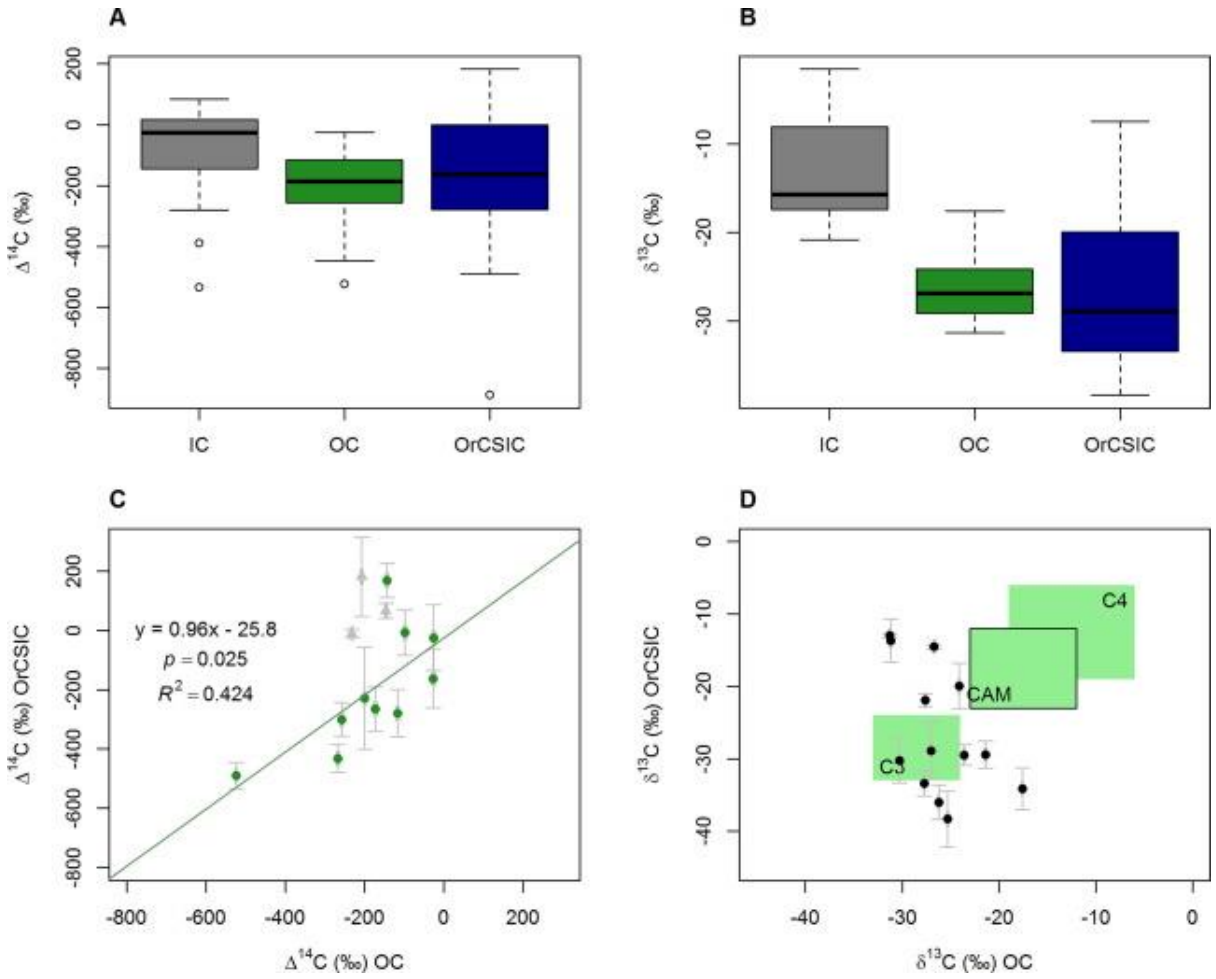

Figure 4 Box and whisker plots of IC, OC, and calculated IC for A) $\Delta^{14}C$ and B) $\delta^{13}C$. Scatter plots of the relationship between OC and OrCSIC for C) $\Delta^{14}C$ where grey triangles represent sites with recent recharge and green samples all other localities and D) $\delta^{13}C$.

In addition to indicating the presence of methanotrophic processes, OrCSIC can also be used to assess the relative contributions of OC to redox processes within the aquifer. In doing this we assess whether shallow or deeper OC is more important – a critical debate for this aquifer (Polizzotto et al., 2008; Lawson et al., 2013; Stuckey et al., 2015b; Richards et al., 2019c). ANOVA tests demonstrate that there is no significant difference between either the concentration of or the $\delta^{13}C$ of OrCSIC in the shallow aquifer (<9 m), mid aquifer (9 to 30 m) and deep aquifer (> 30 m) ($p = 0.15$ and $p = 0.11$ respectively, Figure 5A). However, there is a significant difference in the mean residence times of the OrCSIC ($p = 0.04$) with most of the shallow OrCSIC being post-1950s (or very close to 1950) whilst, in the mid and deep aquifer OrCSIC has a mean (± st. dev.) residence times of 2045 ± 2700 years B.P. (skew = 0.66, n = 5) and 4800 ± 6200 years B.P. (skew = 2.41, n = 6) respectively (Table 9, Figure 5). This shows that the mean residence time of OrCSIC increases with depth and that this happens at all locations. This is in stark contrast with the trend for the mean residence time of OC (e.g. LR01, Table 3).

Whilst the increasing of mean residence time of OrCSIC with depth is consistent with the flow patterns, where older flow paths are deeper than younger paths, the OrCSIC mean residence times predate the oldest flow paths (which are 900 years B.P.) by over 1000 years (Benner et al., 2008). Instead, the mean residence times are much closer to the ages of the sedimentary OC in different sedimentary facies which have mean ages of 1800 ± 400 years B.P. (skew = 1.4, n = 5), 3500 ± 440 years B.P. (skew = -0.62, n = 6) and 6200 ± 3900 years B.P. (skew = -0.62, n = 5) (Magnone et al., 2017).

If substantial proportions of OrCSIC were sourced from the shallow sediments the OrCSIC mean residence times would be close to the maximum flow path age or the age of shallow sedimentary OC (1800 ± 400 years B.P.). That the age is closer to the deeper in-situ sedimentary OC which has ages between 3500 ± 440 years B.P. and 6200 ± 3900 years B.P. indicates that in-aquifer oxidation of sedimentary organic carbon is more likely to be the main source OrCSIC.

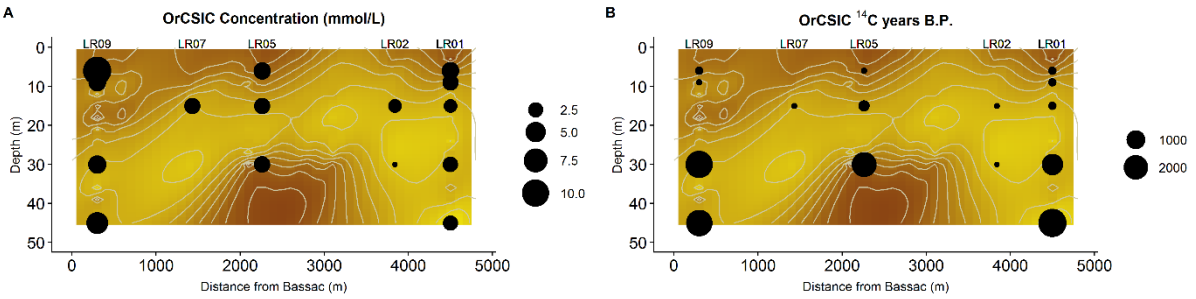

Figure 5 Cross section of T-Sand with OrCSIC concentrations (A) and radiocarbon mean residence times (years B.P.) (B) presented with sedimentary stratigraphy (yellow is sand and brown is clay). Original sedimentary transacted produced by Magnone et al., (2017) reproduced under the terms of an open access Creative Commons Attribution 4.0 International License, details of which may be found at http://creativecommons.org/licenses/by/4.0/.

5) Conclusions

This study has developed and applied a new approach to radiocarbon correction for IC in groundwater enabling the mean residence time of organic sourced IC (OrCSIC, i.e. inorganic carbon which comes from the oxidation of OC) to be calculated. This is an important measurement given that oxidation of organic carbon in redox reactions controls the lability of many contaminants and OrCSIC is a key by-product of such reactions. The method uses $^{87}Sr/^{86}Sr$ coupled with Ca/Na and Mg/Na to calculate the relative proportion of different end-members (e.g. connate water, seawater, soil flux, mineral dissolution etc.) contributing to groundwater solute compositions, including IC. Once the concentrations of IC derived from each source are calculated, a correction is applied, using *a priori* values of end-member mean residence times, resulting in the mean residence time of OrCSIC. The value of this approach is demonstrated with results from the test site and which highlight the importance of deep in-aquifer oxidation of sedimentary OC as a source of OrCSIC, in contrast to

previous studies which have focussed on shallow oxidation processes. The results also hint at the presence of methanotrophic signatures indicating that thermally mature sedimentary OC, known to be present, could be an important source of OrCSIC here as well – a hypothesis that is worth further research. Most critically, however, the results highlight how this new method of interpreting groundwater inorganic radiocarbon data is far more subtle that conventional bulk tracing approaches and can help facilitate better understanding contaminant-controlling redox histories of groundwater.

6) Abbreviations

EM-carbonate = carbonate end-member

EM-recharge = reacharge end-member

EM-silicate = silicate end-member

IC = inorganic carbon

OC = organic carbon

OrCSIC = organic carbon sourced inorganic carbon (*i.e.* inorganic carbon originating from the oxidation of organic carbon)

p = Student's p-value

7) Acknowledgements

We thank three anonymous reviewers for their extremely detailed reviews which have greatly improved the manuscript. This work was supported by a NERC Standard Research Grant (NE/J023833/1) to DP, BvD and Chris J. Ballentine (University of Oxford), a NERC PhD studentship (NE/L501591/1) and University of Manchester President's Doctoral Scholarship both awarded to DM, and a Leverhulme Early Career Fellowship (ECF2015-657) to LR. Radiocarbon analysis was supported by the NERC Radiocarbon Facility NRCF010001 (allocation numbers 1835.0714 and 1906.0714). Strontium analysis was supported with a NERC Isotope Geochemistry Facility grant (IP-1589-1115). The authors thank Dr Michael Lawson (ExxonMobil Upstream Research Company, Houston, Texas, 77019, USA) for advanced access to a manuscript on a similar topic conducted in the same region. We thank Chansopheaktra Sovann (Royal University of Phnom Penh) and Chivuth Kong (Royal University of Agriculture, Phnom Penh) for their assistance and invaluable local knowledge during fieldwork and gratefully recognise the hard work of our drilling team led by Hok Meas as well as the field assistants during our water sampling campaigns (Pheary Meas, Teyden Sok and Yut Yann from the Royal University of Agriculture, Cambodia, and Chhengngunn Aing and Zongta Sang from the Royal

University of Phnom Penh, Cambodia, Dina Kuy from Resources Development International – Cambodia). We thank Lori Frees and Lori Allen (both formerly Resources Development International – Cambodia) whose support and laboratory co-ordination was invaluable during the fieldwork and we thank Resources, Development International – Cambodia for allowing us to use their laboratory and other local assistance. Paul Lythgoe (The University of Manchester) is gratefully thanked for conducting the ICP-MS analysis. We acknowledge the hard work of Francis Elliott (NERC Radiocarbon Facility, UK)and other staff at the SUERC AMS Laboratory for all other radiocarbon analysis. Thanks also are due to Dr Karen Theis (The University of Manchester) for help undertaking sequential extractions particularly carrying out digestions with hydrofluoric acid. Prof. Philippe Négrel (BRGM) and Dr Stephen Boult (The University of Manchester) are thanked for their feedback and suggestions on an early draft of this manuscript.

8) Declaration of interests

Declarations of interest: none.

9) References

Aggarwal P. K., Basu a R., Poreda R. J., Kulkarni K. M., Froehlich K., Tarafdar S. a, Ali M., Ahmed N., Hussain A., Rahman M. and Ahmed S. R. (2000) Isotope Hydrology of Groundwater in Bangladesh: Implications for Characterization and Mitigation of Arsenic in Groundwater. *Int. At. Energy Agency, Austria*, 61.

Allègre C., Dupré B., Négrel P. and Gaillardet J. (1996) Sr-Nd-Pb isotope systematics in Amazon and Congo River systems: constraints about erosion processes. *Chem. Geol.* **131**, 93–112.

Anderson E. C., Libby W. F., Weinhouse S., Reid A. F., Kirshenbaum A. D. and Grosse A. V. (1947) Natural radiocarbon from cosmic radiation. *Phys. Rev.* **72**, 931–936.

Appelo C. A. J. and Postma D. (2005) *Geochemistry, groundwater and pollution. Leiden, Balkema.*, A.A. Balkema Publishers, Great Britain.

Ascott M. J., Gooddy D. C., Wang L., Stuart M. E., Lewis M. A., Ward R. S. and Binley A. M. (2017) Global patterns of nitrate storage in the vadose zone. *Nat. Commun.* **8**, 1416.

Benner S. G., Polizzotto M. L., Kocar B. D., Ganguly S., Phan K., Ouch K., Sampson M. and Fendorf S. (2008) Groundwater flow in an arsenic-contaminated aquifer, Mekong Delta, Cambodia. *Appl. Geochemistry* **23**, 3072–3087.

Bentley R. A. (2006) Strontium isotopes from the earth to the archaeological skeleton: A review. *J. Archaeol. Method Theory* **13**, 135–187.

Bethke C. M. and Johnson T. M. (2008) Groundwater Age and Groundwater Age Dating. *Annu. Rev. Earth Planet. Sci.* **36**, 121–152.

Bethke C. M. and Johnson T. M. (2002) Paradox of groundwater age. *Geology* **30**, 107–110.

Bickle M. J., Bunbury J., Chapman H. J., Harris N. B. W., Fairchild I. J. and Ahmad T. (2003) Fluxes of Sr into the headwaters of the Ganges. *Geochim. Cosmochim. Acta* **67**, 2567–2584.

Bickle M. J., Chapman H. J., Bunbury J., Harris N. B. W., Fairchild I. J., Ahmad T. and Pomiès C. (2005) Relative contributions of silicate and carbonate rocks to riverine Sr fluxes in the headwaters of the Ganges. *Geochim. Cosmochim. Acta* **69**, 2221–2240.

Bickle M. J., Harris N. B. W., Bunbury J. M., Chapman H. J., Fairchild I. J. and Ahmad T. (2001) Controls on the 87Sr/86Sr ratio of carbonates in the Garhwal Himalaya, headwaters of the Ganges. *J. Geol.* **109**, 737–753.

Birck J. L. (1986) Precision K-Rb-Sr isotopic analysis: Application to Rb-Sr chronology. *Chem. Geol.* **56**, 73–83.

Broecker W. S. (2010) Radiocarbon. In *Radioactive Geochronometry* (eds. H. D. Holland and K. K. Turekian). Elsevier. pp. 251–268.

Bryant C. L., Henley S. F., Murray C., Ganeshram R. S. and Shanks R. (2013) Storage and hydrolysis of sewater samples for inorganic carbon isotope analysis. *Radiocarbon* **55**, 401–409.

Cartwright I. (2010) Using groundwater geochemistry and environmental isotopes to assess the correction of 14C ages in a silicate-dominated aquifer system. *J. Hydrol.* **382**, 174–187. Available at: https://www.sciencedirect.com/science/article/pii/S0022169409008269 [Accessed April 30, 2019].

Cartwright I., Hannam K. and Weaver T. R. (2007) Constraining flow paths of saline groundwater at basin margins using hydrochemistry and environmental isotopes: Lake Cooper, Murray Basin, Australia. *Aust. J. Earth Sci.* **54**, 1103–1122. Available at: http://www.tandfonline.com/doi/abs/10.1080/08120090701615741 [Accessed April 30, 2019].

Chatterjee J. and Singh S. K. (2012) 87Sr/86Sr and major ion composition of rainwater of Ahmedabad, India: Sources of base cations. *Atmos. Environ.* **63**, 60–67.

690 Cheng M., You C., Lin F. and Chung C. (2010) Seasonal variation in long-range transported dust to a
691 subtropical islet offshore northern Taiwan: chemical composition and Sr isotopic evidence in
692 rainwater. *Atmos. Environ.*

693 Coetsiers M. and Walraevens K. (2009) A new correction model for 14C ages in aquifers with
694 complex geochemistry - Application to the Neogene Aquifer, Belgium. *Appl. Geochemistry* **24**,
695 768–776.

696 Colin C., Turpin L., Blamart D., Frank N., Kissel C. and Duchamp S. (2006) Evolution of weathering
697 patterns in the Indo-Burman Ranges over the last 280 kyr: Effects of sediment provenance on
698 87 Sr/86 Sr ratios tracer. *Geochemistry, Geophys. Geosystems* **7**.

699 Coplen T. (1994) Reporting of stable hydrogen, carbon, and oxygen isotopic abundances (Technical
700 Report). *Pure Appl. Chem.*

701 Day M. B., Hodell D. A., Brenner M., Curtis J. H., Kamenov G. D., Guilderson T. P., Peterson L. C.,
702 Kenney W. F. and Kolata A. L. (2011) Middle to late Holocene initiation of the annual flood
703 pulse in Tonle Sap Lake, Cambodia. *J. Paleolimnol.* **45**, 85–99.

704 Deer W., Howie R. A. and Zussman J. (2013) *An Introduction to the Rock-Forming Minerals: 3rd*
705 *Edition*., The Mineralogical Society, London.

706 Deines P. (1980) The isotopic composition of reduced organic carbon. In *Handbook of environmental*
707 *isotope geochemistry* pp. 329–406.

708 Dogramaci S. S. and Herczeg A. L. (2002) Strontium and carbon isotope constraints on carbonate-
709 solution interactions and inter-aquifer mixing in groundwaters of the semi-arid Murray Basin,
710 Australia. *J. Hydrol.* **262**, 50–67.

711 Dowling C. B., Poreda R. J. and Basu A. R. (2003) The groundwater geochemistry of the Bengal Basin:
712 Weathering, chemsorption, and trace metal flux to the oceans. *Geochim. Cosmochim. Acta* **67**,
713 2117–2136.

714 Drever J. (1997) *The Geochemistry of Natural Waters*., Prentice Hall.

715 Ettayfi N., Bouchaou L., Michelot J. L., Tagma T., Warner N., Boutaleb S., Massault M., Lgourna Z. and
716 Vengosh A. (2012) Geochemical and isotopic (oxygen, hydrogen, carbon, strontium) constraints
717 for the origin, salinity, and residence time of groundwater from a carbonate aquifer in the
718 Western Anti-Atlas Mountains, Morocco. *J. Hydrol.* **438–439**, 97–111.

719 Fontes J.-C. (1992) Chemical and Isotopic Contraints on 14C Dating of Groundwater. In *Radiocarbon*
720 *After Four Decades* Springer. pp. 242–261.

721 Fontes J.-C. and Garnier J.-M. (1979) Determination of the initial 14C activity of the total dissolved
722 carbon: A review of the existing models and a new approach. *Water Resour. Res.* **15**, 399–413.

723 Ford D. C. and Williams P. (2013) *Karst hydrogeology and geomorphology*., Wiley.

724 Freeman S. P. H. T., Dougans A., McHargue L., Wilcken K. M. and Xu S. (2008) Performance of the
725 new single stage accelerator mass spectrometer at the SUERC. *Nucl. Instruments Methods*
726 *Phys. Res. Sect. B Beam Interact. with Mater. Atoms* **266**, 2225–2228.

727 van Geen A., Zheng Y., Stute M. and Ahmed K. M. (2003) Comment on "Arsenic Mobility and
728 Groundwater Extraction in Bangladesh" (II). *Science (80-.).* **300**, 584; author reply 584.

729 Geyh M. A. (2000) An overview of 14C Analysis in the Study of Groundwater. *Radiocarbon* **42**, 99–
730 114.

731 Gleeson T., Befus K. M., Jasechko S., Luijendijk E. and Cardenas M. B. (2015) The global volume and
732 distribution of modern groundwater. *Nat. Geosci.* **9**, 161–167.

733 Godwin H. (1962) Half-life of Radiocarbon. *Nature* **195**, 984.

734 Gupta A. (2009) Geology and Landforms of the Mekong Basin. *The Mekong*, 29–51. Available at:
735 https://www.sciencedirect.com/science/article/pii/B9780123740267000036 [Accessed March
736 6, 2019].

737 Han G., Wu Q. and Tang Y. (2011) Acid rain and alkalization in southwestern China: chemical and
738 strontium isotope evidence in rainwater from Guiyang. *J. Atmos. Chem.* **68**, 139–155.

739 Harrington G. A., Cook P. G. and Herczeg A. L. (2002) Spatial and Temporal Variability of Ground
740 Water Recharge in Central Australia: A Tracer Approach. *Ground Water* **40**, 518–527. Available
741 at: http://doi.wiley.com/10.1111/j.1745-6584.2002.tb02536.x [Accessed April 30, 2019].

742 Harrington G. A. and Herczeg A. L. (1998) *Estimating groundwater 14C ages in the arid Ti-Tree Basin,*
743 *Central Australia: Use of 87Sr/86Sr to constrain sources of inorganic carbon*., Available at:
744 https://inis.iaea.org/collection/NCLCollectionStore/_Public/30/025/30025848.pdf?r=1&r=1
745 [Accessed March 20, 2019].

746 Harrington G. A. and Herczeg A. L. (2003) The importance of silicate weathering of a sedimentary
747 aquifer in arid Central Australia indicated by very high 87Sr/86Sr ratios. *Chem. Geol.* **199**, 281–

292. Available at: https://www.sciencedirect.com/science/article/pii/S0009254103001281 [Accessed April 30, 2019].

Harvey C. F., Swartz C. H., Badruzzaman A. B. M., Keon-Blute N., Yu W., Ali M. A., Jay J., Beckie R., Niedan V., Brabander D., Oates P. M., Ashfaque K. N., Islam S., Hemond H. F. and Ahmed M. F. (2002) Arsenic Mobility and Groundwater Extraction in Bangladesh. *Science (80-.).* **298**, 1602–1606.

Hengl T., de Jesus J. M., MacMillan R. A., Batjes N. H., Heuvelink G. B. M., Ribeiro E., Samuel-Rosa A., Kempen B., Leenaars J. G. B., Walsh M. G. and Gonzalez M. R. (2014) SoilGrids1km — Global Soil Information Based on Automated Mapping ed. B. Bond-Lamberty. *PLoS One* **9**, e105992. Available at: http://dx.plos.org/10.1371/journal.pone.0105992 [Accessed February 10, 2017].

Hengl T., Mendes de Jesus J., Heuvelink G. B. M., Ruiperez Gonzalez M., Kilibarda M., Blagotić A., Shangguan W., Wright M. N., Geng X., Bauer-Marschallinger B., Guevara M. A., Vargas R., MacMillan R. A., Batjes N. H., Leenaars J. G. B., Ribeiro E., Wheeler I., Mantel S. and Kempen B. (2017) SoilGrids250m: Global gridded soil information based on machine learning. *PLoS One* **12**, e0169748. Available at: http://dx.plos.org/10.1371/journal.pone.0169748 [Accessed February 16, 2017].

Hua Q., Barbetti M. and Rakowski A. Z. (2013) Atmospheric Radiocarbon for the Period 1950–2010. *Radiocarbon* **55**, 2059–2072. Available at: https://www.cambridge.org/core/product/identifier/S0033822200048979/type/journal_article [Accessed March 5, 2019].

Ingerson E. and Pearson F. (1964) Estimation of age and rate of motion of ground water by the 14C method. *Recent Res. Fields Hydrosphere, Atmos. Nucl. Chem.*, 263–283.

Islam F. S., Gault A. G., Boothman C., Polya D. A., Charnock J. M., Chatterjee D. and Lloyd J. R. (2004) Role of metal-reducing bacteria in arsenic release from Bengal delta sediments. *Nature* **430**, 68–71.

Jacobson A. and Blum J. (2000) Ca/Sr and 87Sr/86Sr geochemistry of disseminated calcite in Himalayan silicate rocks from Nanga Parbat: Influence on river-water chemistry. *Geology* **28**, 463–466.

Jasechko S., Perrone D., Befus K. M., Bayani Cardenas M., Ferguson G., Gleeson T., Luijendijk E., McDonnell J. J., Taylor R. G., Wada Y. and Kirchner J. W. (2017) Global aquifers dominated by fossil groundwaters but wells vulnerable to modern contamination. *Nat. Geosci.* **10**, 425–429.

779 Jin Z., Bickle M., Chapman H., Yu J., An Z. and Wang S. (2011) Ostracod Mg/Sr/Ca and 87Sr/86Sr
780 geochemistry from Tibetan lake sediments: Implications for early to mid-Pleistocene Indian
781 monsoon and catchment weathering. *Boreas* **40**, 320–331.

782 Kamenov G., Brenner M. and Tucker J. (2009) Anthropogenic versus natural control on trace element
783 and Sr–Nd–Pb isotope stratigraphy in peat sediments of southeast Florida (USA),∼ 1500 AD to
784 present. *Geochim. Cosmochim. Acta* **73**, 3549–3567.

785 Kessler T. J. and Harvey C. F. (2001) *The global flux of carbon dioxide into groundwater*., Available at:
786 http://www.agu.org/pubs/esupp_about.html. [Accessed March 5, 2019].

787 Kiernan K. (2009) Distribution and Character of Karst in the Lao PDR. *Acta Carsologica* **38**. Available
788 at: http://ojs.zrc-sazu.si/carsologica/article/view/137 [Accessed March 6, 2019].

789 Kocar B. D., Polizzotto M. L., Benner S. G., Ying S. C., Ung M., Ouch K., Samreth S., Suy B., Phan K.,
790 Sampson M. and Fendorf S. (2008) Integrated biogeochemical and hydrologic processes driving
791 arsenic release from shallow sediments to groundwaters of the Mekong delta. *Appl.*
792 *Geochemistry* **23**, 3059–3071.

793 de Laeter J. R., Böhlke J. K., De Bièvre P., Hidaka H., Peiser H. S., Rosman K. J. R. and Taylor P. D. P.
794 (2003) Atomic weights of the elements. Review 2000 (IUPAC Technical Report). *Pure Appl.*
795 *Chem.* **75**, 683–800.

796 Lawson M., Polya D. A., Boyce A. J., Bryant C. and Ballentine C. J. (2016) Tracing organic matter
797 composition and distribution and its role on arsenic release in shallow Cambodian
798 groundwaters. *Geochim. Cosmochim. Acta* **178**, 160–177.

799 Lawson M., Polya D. A., Boyce A. J., Bryant C., Mondal D., Shantz A. and Ballentine C. J. (2013) Pond-
800 derived organic carbon driving changes in arsenic hazard found in asian groundwaters. *Environ.*
801 *Sci. Technol.* **47**, 7085–7094.

802 Li X.-D., Liu C.-Q., Harue M., Li S.-L. and Liu X.-L. (2010) The use of environmental isotopic (C, Sr, S)
803 and hydrochemical tracers to characterize anthropogenic effects on karst groundwater quality:
804 A case study of the Shuicheng Basin, SW China. *Appl. Geochemistry* **25**, 1924–1936. Available
805 at: https://www.sciencedirect.com/science/article/pii/S0883292710002295 [Accessed April 30,
806 2019].

807 Liu Z., Colin C., Huang W., Phon Le K., Tong S., Chen Z. and Trentesaux A. (2007) Climatic and tectonic
808 controls on weathering in south China and Indochina Peninsula: Clay mineralogical and

809 geochemical investigations from the Pearl, Red, and Mekong drainage basins. *Geochemistry,*
810 *Geophys. Geosystems* **8**.

811 Magnone D., Richards L. A., Polya D. A., Bryant C., Jones M. and Van Dongen B. E. (2017) Biomarker-
812 indicated extent of oxidation of plant-derived organic carbon (OC) in relation to
813 geomorphology in an arsenic contaminated Holocene aquifer, Cambodia. *Sci. Rep.* **7**.

814 McArthur J., Howarth R. and Bailey T. (2001) isotope stratigraphy: LOWESS version 3: best fit to the
815 marine Sr-isotope curve for 0–509 Ma and accompanying look-up table for deriving numerical
816 age. *J. Geol.* **109**, 155–170.

817 Mossop K. and Davidson C. (2003) Comparison of original and modified BCR sequential extraction
818 procedures for the fractionation of copper, iron, lead, manganese and zinc in soils and
819 sediments. *Anal. Chim. Acta* **478**, 111–118.

820 Nakano T. and Tanaka T. (1997) Strontium isotope constraints on the seasonal variation of the
821 provenance of base cations in rain water at Kawakami, central Japan. *Atmos. Environ.* **31**,
822 4237–4245.

823 Négrel P. (1999) Geochemical study of a granitic area–the Margeride Mountains, France: chemical
824 element behavior and 87Sr/86Sr constraints. *Aquat. Geochemistry* **5**, 125–165.

825 Négrel P., Allegre C. J., Dupre B. and Lewin E. (1993) Erosion Sources Determined By Inversion of
826 Major and Trace-Element Ratios and Strontium Isotopic-Ratios in River Water - the Congo Basin
827 Case. *Earth Planet. Sci. Lett.* **120**, 59–76.

828 Négrel P. and Deschamps P. (1996) Natural and anthropogenic budgets of a small watershed in the
829 Massif Central (France): chemical and strontium isotopic characterization of water and
830 sediments. *Aquat. Geochemistry* **2**, 1–27.

831 Négrel P., Fouillac C. and Brach M. (1997) A strontium isotopic study of mineral and surface waters
832 from the Cézallier (Massif Central, France): implications for mixing processes in areas of
833 disseminated. *Chem. Geol.* **135**, 89–101.

834 Négrel P. and Petelet-Giraud E. (2005) Strontium isotopes as tracers of groundwater-induced oods:
835 the Somme case study (France). *J. Hydrol.* **305**, 99–119.

836 Newsome L., Cleary A., Morris K. and Lloyd J. R. (2017) Long-Term Immobilization of Technetium via
837 Bioremediation with Slow-Release Substrates. *Environ. Sci. Technol.* **51**, 1595–1604.

838 Oliver L., Harris N., Bickle M., Chapman H. and Dise N. (2003) Silicate weathering rates decoupled
839 from the 87 Sr/86 Sr ratio of the dissolved load during Himalayan erosion. *Chem. Geol.* **201**,
840 119–139.

841 Parkhurst D. L. and Appelo C. A. J. (2013) Description of input and examples for PHREEQC version 3.
842 *A Comput. Progr. speciation, batch-reaction, one-dimensional Transp. inverse geochemical Calc.*
843 **Chapter A4**.

844 Pearson F. and Hanshaw B. (1970) *Sources of dissolved carbonate species in groundwater and their*
845 *effects on carbon-14 dating*.,

846 Plummer L. N. and Glynn P. D. (2013) Radiocarbon Dating in Groundwater Systems ed. A.
847 International Atomic Energy Agency. *Isot. Methods Dating Old Groundw.*, 33–89.

848 Polizzotto M. L., Kocar B. D., Benner S. G., Sampson M. and Fendorf S. (2008) Near-surface wetland
849 sediments as a source of arsenic release to ground water in Asia. *Nature* **454**, 505–508.

850 Polya D. A., Richards L. A., Al Bualy A. A. N., Sovann C., Magnone D. and Lythgoe P. (2017)
851 Groundwater sampling , arsenic analysis and risk communication: Cambodia case study. In *Best*
852 *Practice Guide on the Control of Arsenic in Drinking Water* International Water Association. pp.
853 247–256.

854 Ponta G. M. and Aharon P. (2014) Karst geology and isotope hydrology of the upstream section of
855 Nam Hinboun River, Khammouan Province (Central Laos). *Carbonates and Evaporites* **29**, 127–
856 139. Available at: http://link.springer.com/10.1007/s13146-014-0194-5 [Accessed March 6,
857 2019].

858 Ravenscroft P., Brammer H. and Richards K. (2009) *Arsenic Sollution: A Global Synthesis*., Wiley-
859 Blackwell.

860 Richards L. A., Casanueva-Marenco M. J., Magnone D., Sovann C., van Dongen B. E. and Polya D. A.
861 (2019a) Contrasting sorption behaviours affecting groundwater arsenic concentration in Kandal
862 Province, Cambodia. *Geosci. Front.*

863 Richards L. A., Lapworth D. J., Magnone D., Gooddy D. C., Chambers L., Williams P. J., van Dongen B.
864 E. and Polya D. A. (2019b) Dissolved organic matter tracers reveal contrasting characteristics
865 across an arsenic bearing aquifer in Cambodia: A fluorescence spectroscopy study. *Geosci.*
866 *Front.*

867 Richards L. A., Magnone D., Boyce A. J., Casanueva-Marenco M. J., van Dongen B. E., Ballentine C. J.

and Polya D. A. (2018) Delineating sources of groundwater recharge in an arsenic-affected Holocene aquifer in Cambodia using stable isotope-based mixing models. *J. Hydrol.* **557**, 321–334.

Richards L. A., Magnone D., van Dongen B. E., Ballentine C. J. and Polya D. A. (2015) Use of lithium tracers to quantify drilling fluid contamination for groundwater monitoring in Southeast Asia. *Appl. Geochemistry* **63**, 190–202.

Richards L. A., Magnone D., Sovann C., Kong C., Uhlemann S., Kuras O., van Dongen B. E., Ballentine C. J. and Polya D. A. (2017a) High resolution profile of inorganic aqueous geochemistry and key redox zones in an arsenic bearing aquifer in Cambodia. *Sci. Total Environ.* **590**, 540–553.

Richards L. A., Magnone D., Sültenfuß J., Chambers L., Bryant C., Boyce A. J., van Dongen B. E., Ballentine C. J., Sovann C., Uhlemann S., Kuras O., Gooddy D. C. and Polya D. A. (2019c) Dual in-aquifer and near surface processes drive arsenic mobilization in Cambodian groundwaters. *Sci. Total Environ.* **659**, 699–714.

Richards L. A., Sültenfuß J., Ballentine C. J., Magnone D., van Dongen B. E., Sovann C. and Polya D. A. (2017b) Tritium Tracers of Rapid Surface Water Ingression into Arsenic-bearing Aquifers in the Lower Mekong Basin, Cambodia. *Procedia Earth Planet. Sci.* **17**, 845–848.

Richards L. A., Sültenfuß J., Magnone D., Boyce A., Sovann C., Casanueva-Marenco M. J., Ballentine C. J., Dongen B. E. van and Polya D. A. (2016) Age and provenance of groundwater in a shallow arsenic-affected aquifer in the lower Mekong Basin, Kandal Province, Cambodia. In *In Arsenic Research and Global Sustainability: Proceedings of the Sixth International Congress on Arsenic in the Environment (As2016), June 19-23, Stockholm, Sweden* CRC Press. p. 74.

Rowland H. A. L., Pederick R. L., Polya D. A., Pancost R. D., van Dongen B. E., Gault A. G., Vault D. J., Bryant C., Anderson B. and Lloyd J. R. (2007) The control of organic matter on microbially-mediated iron reduction and arsenic release in shallow alluvial aquifers. *Geobiology* **5**, 281–292.

Siebert S., Burke J., Faures J. M., Frenken K., Hoogeveen J., Döll P. and Portmann F. T. (2010) Groundwater use for irrigation - A global inventory. *Hydrol. Earth Syst. Sci.* **14**, 1863–1880.

Slota P., Jull A. J. T., Linick T. W. and Toolin L. J. (1987) Preparation of small samples for 14C accelerator targets by catalytic reduction of CO. *Radiocarbon* **29**, 303–306.

Sovann C. and Polya D. A. (2014) Improved groundwater geogenic arsenic hazard map for Cambodia.

Environ. Chem. **11**, 595–607.

Stuckey J. W., Schaefer M. V., Benner S. G. and Fendorf S. (2015a) Reactivity and speciation of mineral-associated arsenic in seasonal and permanent wetlands of the Mekong Delta. *Geochim. Cosmochim. Acta* **171**, 143–155. Available at: https://www.sciencedirect.com/science/article/pii/S0016703715005311 [Accessed March 5, 2019].

Stuckey J. W., Schaefer M. V, Kocar B. D., Benner S. G. and Fendorf S. (2015b) Arsenic release metabolically limited to permanently water-saturated soil in Mekong Delta. *Nat. Geosci.* **9**, 70–76.

Stuiver M. and Polach H. A. (1977) Reporting of C-14 data–discussion. *Radiocarbon* **19**, 355–363.

Tamers M. A. (1967) Surface-water infiltration and groundwater movement in arid zones of Venezuela, in Isotopes in Hydrology. *Int. At. Energy Agency, Austria*, 339–351.

Tamers M. A. (1970) Validity of Radiocarbon Dates on Terrestrial Snail Shells. *Am. Antiq.* **35**, 94–100.

Tamers M. A. and Scharpenseel H. W. (1970) Sequential sampling of radiocarbon in groundwater, in Isotope Hydrology. *Int. At. Energy Agency, Austria*, 241–256.

Tipper E., Bickle M., Galy A., West A., Pomiès C. and Chapman H. J. (2006a) The short term climatic sensitivity of carbonate and silicate weathering fluxes: insight from seasonal variations in river chemistry. *Geochim. Cosmochim. Acta* **70**, 2737–2754.

Tipper E., Galy A., Gaillardet J., Bickle M., Elderfield H. and Carder E. A. (2006b) The magnesium isotope budget of the modern ocean: constraints from riverine magnesium isotope ratios. *Earth Planet.* **250**, 241–253.

Uhlemann S., Kuras O., Richards L. A., Naden E. and Polya D. A. (2017) Electrical resistivity tomography determines the spatial distribution of clay layer thickness and aquifer vulnerability, Kandal Province, Cambodia. *J. Asian Earth Sci.* **147**, 402–414.

Vogel J. C. (1970) Carbon-14 dating of groundwater, in Isotope Hydrology. *Int. At. Energy Agency, Austria*, 235–237.

Walker M. J. C. (2005) Quaternary dating methods. , 20–23.

WDCPC (2016) World Data Centre for Precipitation Chemistry. *Natl. Ocean. Atmos. Adm.* Available at: http://www.wdcpc.org/.

927 Whiticar M. J. (1999) Carbon and hydrogen isotope systematics of bacterial formation and oxidation
928 of methane. *Chem. Geol.* **161**, 291–314. Available at:
929 https://www.sciencedirect.com/science/article/pii/S0009254199000923#FIG4 [Accessed
930 March 25, 2019].

931 Xu S., Anderson R., Bryant C. and Cook G. (2004) Capabilities of the New SUERC 5MV AMS Facility for
932 14C Dating. *Radiocarbon* **46**, 59–64.

933 Xu Z. and Han G. (2009) Chemical and strontium isotope characterization of rainwater in Beijing,
934 China. *Atmos. Environ.* **43**, 1954–1961.

935